The Perseus OB2 Superbubble and the Taurus-Auriga-California-Perseus Molecular Cloud Loop

Xuepeng Chen (xpchen@pmo.ac.cn)
Purple Mountain Observatory
Weihua Guo
Purple Mountain Observatory https://orcid.org/0000-0002-8589-9611
Jiangcheng Feng
Purple Mountain Observatory
Yang Su
Purple Mountain Observatory https://orcid.org/0000-0002-0197-470X
Yan Sun
Purple Mountain Observatory
Qingzeng Yan
Purple Mountain Observatory
Min Fang
Purple Mountain Observatory
Ji Yang
Purple Mountain Observatory https://orcid.org/0000-0001-7768-7320

Letter

Keywords: planetary science, astronomy, Perseus OB2

Posted Date: March 26th, 2021

DOI: https://doi.org/10.21203/rs.3.rs-226848/v1

The Perseus OB2 Superbubble and the Taurus-Auriga-California-Perseus Molecular Cloud Loop

Xuepeng Chen[1,2*], Weihua Guo[1,2], Jiancheng Feng[1,2], Yang Su[1], Yan Sun[1], Qingzeng Yan[1], Min Fang[1], and Ji Yang[1,2]

[1]*Purple Mountain Observatory & Key Laboratory of Radio Astronomy, Chinese Academy of Sciences, 10 Yuanhua Road, 210023 Nanjing, China*

[2]*School of Astronomy and Space Science, University of Science and Technology of China, Hefei, Anhui 230026, China*

Located at a distance of ~ 300 pc, Perseus OB2 (or Per OB2 for short) is one of the major OB associations in the solar vicinity[1,2], which has blown a supershell with a diameter of $\sim 15^\circ$ seen in the atomic hydrogen line surveys[3–5]. It was long considered that stellar feedback from the Per OB2 association had formed a superbubble that swept up the surrounding interstellar medium into the observed supershell[6]. Here we report the three-dimensional structure of the Per OB2 superbubble, based on wide-field atomic hydrogen and molecular gas (traced by CO) surveys. The measured diameter of the superbubble is ~ 330 pc. Multiple atomic hydrogen shells/loops with expansion velocities of $\sim 10\,\mathrm{km\,s^{-1}}$ are revealed in the superbubble, suggesting a complicated evolution history of the superbubble. Furthermore, the inspections of the morphology, kinematics and timescale of the Taurus-Auriga, California, and Perseus molecular clouds shows that the cloud complex is a super molecular cloud loop circling around and co-expanding with the Per OB2 superbubble. We conclude that the

Taurus-Auriga-California-Perseus loop, the largest star-forming molecular cloud complex in the solar neighborhood, is formed from the feedback of the Per OB2 superbubble.

In order to understand the structure of the Per OB2 superbubble, as well as its relationship with surrounding molecular clouds, we present wide-field images toward the Per OB2 region, based on the data obtained from the atomic hydrogen (HI) 4π survey (HI4PI; ref.[7]) and the CfA-1.2 m ^{12}CO ($J = 1$–0) molecular line survey[8]. Complementary CO ($J = 1$–0) images from the surveys conducted with the Purple Mountain Observatory (PMO) 13.7 m telescope and the Five College Radio Astronomy Observatory (FCRAO) 14 m telescope are also used in this work (see Methods).

Previous HI surveys showed that the emission of the Per OB2 supershell ranges from approximately –10 to +10 km s^{-1} in the local standard of rest (LSR) frame[3–5]. After checking the HI4PI velocity channel maps (see Supplementary Figure 1), we find that the HI gas morphology changes clearly within this velocity range. Figure 1 shows the HI intensity images toward the Per OB2 region, integrated within the velocity ranges of [–6.0, –0.5], [–0.5, +4.5], and [+4.5, +11.0] km s^{-1}, respectively. In the first velocity range (blue range; see Fig. 1a), a cavity centered on the Galactic position of ($l = 166.0°$, $b = –17.0°$) is seen. This cavity, with an angular dimension of $\sim 16° \times 15°$, represents the long known HI supershell around the Per OB2 association[9]. As seen in Fig. 1a (see also channel maps in Supplementary Figure 1), faint concentric shells are detected within the cavity, while dense wall is found to the northeast of the cavity. In the second velocity range (green range; see Fig. 1b), more dense walls are observed around the cavity. Furthermore,

two large curved filaments are detected to the south of the cavity, which emerge from eastern cavity wall and extend to the west. In the last velocity range (red range; see Fig. 1c), these two large filaments appear to merge into one shell to the southeast of the cavity. In the mean velocity field shown in Fig. 1d, these different velocity components together delineate a superbubble, which is extending in the north-south direction.

Figure 2 shows the HI position-velocity (PV) diagrams along different routings across the superbubble (see Fig. 1 for the PV routings). The HI emission of the superbubble is mainly within the velocity range from –6 to +11 $\mathrm{km\,s^{-1}}$ (i.e., the velocity range shown in Figure 1). Cavity-like PV patterns are detected in all the routings, indicating that the superbubble is expanding. Furthermore, spur-like protrusions, spatially coincident with the dense walls/filaments seen in the HI intensity images (see Figure 1), are also detected along the PV diagrams (see Figure 2). As seen in the diagrams, the cavity-like patterns, as well as the protrusions, could be well fitted by ellipses, with the position and velocity radii representing the projected radii and expansion velocities, respectively. Based on the PV diagrams and intensity images, two large HI loops, surrounding the central cavity, can be outlined in the velocity range of [–0.5, +4.5] $\mathrm{km\,s^{-1}}$ (the green range; see Fig. 1b). The large curved filaments detected to the south of the cavity are parts of the two loops. The angular dimensions of the HI loops are roughly $31^\circ \times 21^\circ$ (HI Loop I) and $42^\circ \times 30^\circ$ (HI Loop II), respectively. The derived expansion velocities for the central cavity, HI Loop I, and Loop II are similar with each other ($\sim 10 \pm 1\,\mathrm{km\,s^{-1}}$). We note that much fainter protrusions are also seen in the PV diagrams (see Figure 2), which are spatially coincident with the faint concentric shells detected in the intensity images (see HI velocity channel maps and Figure 1). Further high sensitivity

and angular resolution HI observations are needed to study these diffuse structures.

Giant molecular clouds (GMCs), generally with size > 100 pc and mass $> 10^5\ M_\odot$, are the primary reservoirs of cold, dense, and star-forming molecular gas in the Milky Way[10] and nearby galaxies[11]. However, the formation mechanisms of GMCs are not well understood yet[12,13]. The feedback from OB associations can drive converging flows to accumulate atomic hydrogen gas (i.e., super-shells and -bubbles) to form molecular clouds[14–16], which has been observed in a few distant supershells in the Galaxy[17–20]. For solar neighborhood conditions, nevertheless, it was generally considered that the maximum mass of molecular clouds, formed by stellar feedback, is limited to be a few times of $10^4\ M_\odot$ (ref.[12]).

The Taurus-Auriga, California, and Perseus Clouds, with a total gas mass of $\sim 2 \times 10^5\ M_\odot$, is the largest star-forming molecular cloud complex in the solar vicinity[8,21]. Surrounding the Per OB2 association, these well-known clouds are located at different distances along the line-of-sight[22]. The Taurus Cloud, at a distance of $\sim$140 pc, is in the foreground of Per OB2, while the California Cloud, at a distance of ~ 470 pc, is in the background of Per OB2. The distance of the Perseus Cloud is estimated to be ~ 290 pc, and it is thus immediately at the front edge of the association. It is of importance to study the relationship between these molecular clouds and the Per OB2 superbubble.

As seen in the CO velocity channel maps (Supplementary Figure 2), the molecular gas observed in the Taurus-Auriga, California, and Perseus Clouds is spatially co-moving with the HI shells of the Per OB2 superbubble – either lying along the dense walls of the cavity (for the Cal-

ifornia and Perseus Clouds; see Supplementary Figure 3) or well embedded within them (for the Taurus-Auriga Cloud). This kind of CO-HI co-moving morphology is generally regarded as a key indicator for the molecular clouds forming as coherent parts of atomic shells[20].

In the CO velocity-integrated intensity images, the Taurus-Auriga, California, and Perseus Clouds consist of a super molecular cloud loop (see Figure 3). We extract an PV diagram along the ridge of the loop to inspect its kinematics (see Figure 4). The PV diagram shows that the molecular cloud loop is expanding with a velocity of $\sim 10\,\mathrm{km\,s^{-1}}$, with respect to a systemic velocity of $\sim 1\,\mathrm{km\,s^{-1}}$. In this expanding loop, the California Cloud is blue-shifted, the Taurus Cloud is red-shifted, while the Perseus Cloud appears at the tangential portion of the loop. This expansion picture is consistent with the distances of these clouds regarding to the Per OB2 association. A similar PV diagram is extracted along the HI Loop I (see Figure 4). The comparison between the CO and HI PV diagrams indicates that the Taurus-Auriga-California-Perseus loop is expanding together with the Per OB2 superbubble.

The CO velocity fields of the molecular clouds provide further evidence for physical relation between the molecular cloud loop and the Per OB2 superbubble (see Supplementary Figure 5). As seen in the velocity field images, systematic velocity gradient is observed along the Perseus Cloud (see also the CO PV diagram in Figure 4). Furthermore, systematic velocity gradients are observed perpendicularly to the filamentary structures found in the California and Taurus Clouds, and the directions of the velocity gradients toward the two filamentary structures are opposite with each other. The velocity fields suggest that the California Cloud (in the background of Per OB2),

Taurus Cloud (in the foreground of Per OB2), and Perseus Cloud (nearby Per OB2) are all pushed by the expanding Per OB2 superbubble. In this picture, the diameter of the Per OB2 superbubble can then be estimated to be 330 pc in the direction from the Taurus Cloud ($d \sim 140$ pc) to the California Cloud ($d \sim 470$ pc).

The kinetic age of an expanding bubble can be derived by

$$t_{\rm kin}\ ({\rm Myr}) = 0.6 \frac{R_{\rm bubble}}{V_{\rm exp}}, \quad (1)$$

where $R_{\rm bubble}$ is the radius of the bubble in pc and $V_{\rm exp}$ is the expansion velocity in km s^{-1} (ref.[14]). Adopting a radius of 165 pc and an expansion velocity of 10 km s^{-1}, the estimated kinetic age of the Per OB2 superbubble is roughly 10 Myr. This is consistent with the age estimated to the Per OB2 association (≤ 15 Myr; refs.[2,6,23]), comparable with the average lifetime of the GMCs in nearby Galaxies (~ 10 Myr; ref.[24]), but much longer than the typical lifetime of molecular clouds in the solar neighborhood (a few Myr; ref.[15]). It indicates that the Taurus-Auriga-California-Perseus loop is not a pre-existing molecular cloud complex around the Per OB2 superbubble.

Using the standard method[25], the energy $E_{\rm E}$ needed to open an interstellar bubble could be derived by

$$E_{\rm E}\ ({\rm erg}) = 5.3\ \times\ 10^{43}\ n_{\rm gas}^{1.12}\ R_{\rm bubble}^{3.12}\ V_{\rm exp}^{1.4}, \quad (2)$$

where $n_{\rm gas}$ is the density of ambient gas in cm^{-3}, $R_{\rm bubble}$ is the radius of the bubble in pc, and $V_{\rm exp}$ is the expansion velocity in km s^{-1}. Based on the HI line observations, the density $n_{\rm gas}$ of the interstellar gas surrounding Per OB2 is estimated to be ~ 1 cm^{-3} (see Methods). Adopting $R_{\rm bubble} = 165$ pc and $V_{\rm exp} = 10$ km s^{-1}, the estimated $E_{\rm E}$ is $\sim 1.1 \times 10^{52}$ erg for opening the

Per OB2 superbubble, which is much larger than the typical energy provided by a single supernova (SN) explosion ($E_{\rm SN} \sim 10^{51}$ erg). This is not surprised because superbubbles could be produced by combined stellar feedbacks from a group of massive stars[26] and/or repeated stellar feedbacks from multiple star formation episodes in the OB associations[14]. Numerical studies show that superbubbles retain only $\leq 10\%$ of the energy of an SN explosion[28]. On the other hand, ionizing radiation and stellar wind from a massive star can each provide a few 10^{50} erg during the H II and main-sequence phases, respectively[14,27]. Assuming that a massive star releases in total 10^{51} erg energy into a bubble during its whole lifetime (including ionizing radiation, stellar wind and eventually an SN), the formation of the Per OB2 superbubble should require roughly 11 OB stars. There are several known massive stars in the Per OB2 association (refs.[1,2]; see Figure 1a), such as 38 Per (B1III), ζ Per (B1Ib), 40 Per (B0.5V), and ξ Per (O7IIIe). We note that evidences of SN explosions were also found in Per OB2 (see Methods).

Based on the evidences from morphology, kinematics and timescale, we conclude that the Taurus-Auriga-California-Perseus molecular cloud loop is formed by the feedback of the Per OB2 superbubble. Compared with other well-studied superbubbles in the solar vicinity (see Methods), this super molecular cloud loop is unique, providing us a crucial sample to study the connection between HI superbubbles and molecular clouds. Furthermore, the multiple shells observed in the Per OB2 superbubble implies a complicated evolution history, which could be produced by repeated stellar feedback in the OB association. Suggested by the structures of the central cavity, HI Loops I and II, we consider that there are three star formation epochs in the Per OB2 association. Given a kinetic age of 10 Myr estimated above, the mean star formation epoch is roughly 3 Myr,

which favors the scenario of rapid star formation[15,29]. This is also consistent with the observations toward Per OB, in which three stellar groups with different ages ($\sim$ 1 Myr, 1-5 Myr, and 5-10 Myr, respectively) are found[23]. The well-studied young stellar objects in the Taurus Cloud (with an age of $\sim$ 1-2 Myr; ref.[15]), as well as young clusters found in the California Cloud (the LkHα 101 cluster with an age of $\sim$ 1 Myr; ref.[30]) and Perseus Cloud (e.g., the IC 348 cluster with an age of 1-3 Myr; ref.[6,15]) are likely formed in the last star formation epoch.

Methods

Multi-wavelength observational data. We retrieved the HI line data from the HI4PI (ref.[7]) survey toward the Per OB2 region. The HI4PI survey is based on data from the recently completed first coverage of the Effelsberg-Bonn HI Survey (EBHIS; ref.[31]) and from the third revision of the Galactic All-Sky Survey (GASS; ref.[32]). The HI4PI survey toward the northern sky was performed with the Effelsberg 100-m telescope in Germany and the southern sky performed with the 64-meter Parkes radio telescope in Australia. The released HI4PI data have a velocity resolution of $\sim 1.29\,\mathrm{km\,s^{-1}}$ with an angular resolution of $\sim 16.2'$, while the typical rms noise of the line data is about 43 mK. Supplementary Figure 1 shows the HI line velocity channel maps within the velocity range from $-14\,\mathrm{km\,s^{-1}}$ to $+15\,\mathrm{km\,s^{-1}}$, where the detailed HI gas structure and kinematics of the Per OB2 association can be seen.

Wide-field ^{12}CO $J = 1$–0 line data toward the Taurus-Auriga-California-Perseus cloud complex were from the CfA-1.2 m CO survey toward the Galactic plane[8]. The FWHM beam size in the CfA-1.2 m CO survey is roughly $8'$, while the velocity resolution is $\sim 1.3\,\mathrm{km\,s^{-1}}$. We also retrieved complementary FCRAO 14 m ^{12}CO $J = 1$–0 data for the Taurus Cloud[33,34] and Perseus Cloud[35]. The FWHM beam size in the FCRAO ^{12}CO observations is $\sim 45''$, while the velocity resolution is $\sim 0.065\,\mathrm{km\,s^{-1}}$.

Further CO $J = 1$–0 line observations toward the California Cloud is part of the Milky Way Imaging Scroll Painting (MWISP) project for investigating the nature of the molecular gas along the northern Galactic Plane, using the PMO 13.7 m telescope in Qinghai, China. The CO observa-

tions were made from February 2012 to May 2014. The nine-beam Superconducting Spectroscopic Array Receiver (SSAR; ref.[36]) was working as the front end in sideband separation mode. Three CO (J = 1–0) lines were simultaneously observed, ^{12}CO at the upper sideband (USB) and two other lines, ^{13}CO and C^{18}O, at the lower sideband (LSB). The total of pointing and tracking errors is about 5″, and the half-power beam width (HPBW) is $\sim$55″ (^{12}CO line). A Fast Fourier Transform (FFT) spectrometer with a total bandwidth of 1000 MHz and 16,384 channels was used as the back end. The corresponding velocity resolutions were $\sim$0.16 km s^{-1} for the ^{12}CO line and $\sim$0.17 km s^{-1} for both the ^{13}CO and C^{18}O lines. The average rms noises of all final spectra are about 0.5 K for ^{12}CO and about 0.3 K for ^{13}CO and C^{18}O. All data were reduced using the GILDAS package (see https://www.iram.fr/IRAMFR/GILDAS/). The ^{12}CO and ^{13}CO data are used in this work. The C^{18}O data, as well as a more detailed analysis toward the California Cloud, will be presented in other work (Guo et al. in preparation).

The CO images of the Taurus-Auriga-California-Perseus Clouds. Supplementary Figure 2 shows the CfA-1.2 m CO velocity channel maps. As seen in the channel maps, the CO emission from the Taurus-Auriga-California-Perseus cloud complex ranges from roughly -9 km s^{-1} to $+11$ km s^{-1}. Compared with co-moving HI gas of the Per OB2 superbubble, the California Cloud (from –9 to 0 km s^{-1}; see also Supplementary Figure 3a) is embedded in the dense wall to the north and northeast of the central cavity, the Perseus Cloud (from 0 to 11 km s^{-1}; see Supplementary Figures 3b & 3c) is embedded in the western wall, while the Taurus-Auriga Cloud (from 2 to 9 km s^{-1}; see Supplementary Figures 3b & 3c) is mainly located in the front of the cavity.

Supplementary Figure 4 shows the CfA 1.2 m CO velocity-integrated intensity images, in

which the Taurus-Auriga, California, and Perseus Clouds consist of a super molecular cloud loop. The red line shows the ridgeline along the loop, which is defined by the DisPerSE algorithm, a method for identifying filamentary structure in the interstellar medium[37]. Different color polygons in Supplementary Figure 4 show mapping regions in the FCRAO 14 m and PMO 13.7 m CO observations toward the Taurus (red rectangle), Perseus (green polygon) and California (blue polygon) Clouds, respectively. Compared with the CfA 1.2 m CO results, these clouds appear to have double-velocity components in the higher sensitivity CO observations. In the Taurus Cloud, a few faint CO clumps is found in the velocity range of [–4.0, –2.5] km s^{-1} (see Supplementary Figure 4a). In the California Cloud, strong CO emission is observed in the velocity range of [4.0, 6.5] km s^{-1} (see Supplementary Figure 4b). In Perseus, clear CO emission is detected in the velocity range of [–4.0, –0.5] km s^{-1} (see Supplementary Figure 4c). We note that the Taurus-Auriga, California, and Perseus Clouds are far away from the Galactic Plane, and therefore the possibility of random distributions of these cloud clumps is small. After adding these velocity components in the CfA 1.2 m CO PV diagram (see Figure 4), the expansion the super molecular cloud loop can be further confirmed.

Supplementary Figure 5 shows the CO velocity fields for the molecular cloud loop. Systematic velocity gradient is observed along the Perseus Cloud. For the Taurus Cloud (in the foreground of Per OB2), systematic velocity gradient, perpendicular to the B211/B212 filament, was observed in the FCRAO CO images[38], which was explained by the converging flows due to the expansion of the Per OB2 supershell[39]. For the California Cloud (in the background of Per OB2), similar systematic velocity gradient is also detected, which is perpendicular to a large-scale filament revealed

in the MWISP CO observations (Guo et al. in prep.).

The gas density of the Per OB2 superbubble. By integrating HI spectroscopic data in velocity, one can infer the $N_{\rm HI}$ column densities by

$$N_{\rm HI}\,[{\rm cm^{-2}}] = 1.823\,\times\,10^{18}\,\int T_{\rm B}(v){\rm d}v\,[{\rm K\,km\,s^{-1}}], \tag{3}$$

where $T_{\rm B}(v)$ is the brightness temperature profile of the HI gas[40]. And then, the density $n_{\rm gas}$ can be estimated from the radius and column density of the bubble by

$$n_{\rm gas}\;=\;\frac{3N_{\rm shell}}{R_{\rm bubble}}, \tag{4}$$

where $N_{\rm shell}$ is the column density measured at the shell of the bubble[41]. The measured column density of the shells toward the Per OB2 superbubble is about $100\,{\rm K\,km\,s^{-1}}$ or $1.823\times10^{20}\,{\rm cm^{-2}}$, and the estimated volume density is $\sim1\,{\rm cm^{-3}}$ (adopting a radius of 165 pc), which is consistent with the mean volume density observed in the solar neighborhood[42].

Supernovae in the Per OB2 association. The O7 III star ξ Per, the illuminating source of the California Nebula, is a high-velocity star running-away from the Per OB2 association (see Figure 1a). It was long suggested that ξ Per was expelled by an SN explosion of an even more massive companion[43]. The high-mass X-ray binary, X Per, provides the evidence for the other SN explosion in the Per OB2 association. More recently, a middle-age (~0.54 Myr) fast-moving pulsar PSR J0357+3205 was discovered in the Per OB2 region[44] (see Figure 1a). According to its proper motion and estimated age, it started moving from the center of the Per OB2 superbubble. It may provide the evidence for another SN explosion in Per OB2, although the distance of this pulsar remains large uncertainties, ranging from ~200 pc to ~900 pc. It is of interest to search for more

candidates SN remnant (e.g., pulsars and/or non-thermal radio shells) in the Per OB2 region in the further observations.

Comparisons with other well-studied superbubbles. A few superbubbles were found around OB associations in the solar vicinity[1,45]. The Scorpius-Centaurus (or Sco-Cen for short) association, spreading across the fourth quadrant Galactic plane, is the nearest OB association to the Sun. Large loop-like structures and shells, most clearly seen in the HI observations, were observed toward the Sco-Cen association[46–48]. These loops and shells outline an elongated superbubble enclosing the entire association[48]. A relatively smaller HI bubble, with a diameter of ~ 65 pc, was observed around the Upper Sco subgroup. The filamentary molecular cloud ρ Ophiuchus is seen in the southeast gap of the bubble, while the other filamentary molecular cloud Lupus I is seen on the western boundary of the bubble[47,48]. Observations suggested that both molecular clouds have originated from the interaction of this bubble with ambient interstellar medium[47,48].

To the south of Per OB2 is the well-known Orion-Eridanus superbubble[49], with a size of about 140 pc $\times$ 300 pc, opened by the Orion OB1 association[50,51]. Recent studies suggested a series of nested shells superimposed along the line of sight in this superbubble[52,53]. Two super loops, the Barnard's Loop and Eridanus Loop, are located at the far and near ends of the superbubble, respectively. Nevertheless, the two loops are mainly traced by Hα emission. The well-studied filamentary GMCs, Orion A and B, the nearest massive star-forming regions, on the other hand, are located in the interior of the superbubble[51].

IRAS survey showed a super ($\sim 7.5^\circ$ in radius or ~ 60 pc at 450 pc) ring-like structure around

the Vela OB2 association[54], which is named as IRAS Vela Shell (IVS). The IVS is mainly seen in the dust and radio continuum, as well as neutral hydrogen[55]. A large molecular cloud complex along the Galactic plane, the so-called Vela Molecular Ridge (VMR), was found to the (Galactic) north of the IVS[56,57]. Further observations suggested that parts of the VMR, at a distance of $\sim 700 \pm 200$ pc, are associated with the IVS[58].

The Cygnus superbubble is an extended $18^\circ \times 13^\circ$ strong X-ray emission region, approximately centered on the Cygnus OB2 association[59,60]. However, it is still unclear that the superbubble is a real shell[61] or a structure resulted from a projection effect due to the emission from several separate features along the line of sight[60,62]. In the wide-field HI and CO observations, no bubble-like structure was found to be spatially coincident with the Cygnus X-ray superbubble[62].

Compared with above superbubbles, the Cepheus Bubble[17,63] and Carina Flare[18,64], show more similar pictures as seen in the Per OB2 superbubble. For the two superbubbles, HI observations showed well-defined shell structure, while CO observations found that molecular clouds are well distributed along the HI shells, outlining a ring-like morphology. Furthermore, intense star formation activities were observed in both molecular super-rings. Supplementary Table 1 lists the basic parameters for these well-studied superbubbles, together with the result of the Per OB2 superbubble in this work.

Data availability. The HI4PI HI and CfA 1.2 m CO line data are publicly available online. CO data that support the plots within this paper and other findings of this study are available from the corresponding author upon reasonable request.

1. de Zeeuw, P. T., Hoogerwerf, R., de Bruijne, J. H. J., Brown, A. G. A., Blaauw, A. A HIPPARCOS census of the nearby OB associations. *Astron. J.* **117,** 354-399 (1999).

2. Belikov, A. N., Kharchenko, N. V., Piskunov, A. E., Schilbach, E., Scholz, R.-D. Study of the Per OB2 star forming complex. II. Structure and kinematics. *Astron. Astrophys.* **387,** 117-128 (2002).

3. Sancisi, R. Expanding shells of neutral hydrogen as birthplaces of stellar associations. In IAU Symp. 60 (ed. Kerr, F. J. & Simonson, S. C.) 115-128 (Dordrecht: Reidel, 1974).

4. Heiles, C. HI shells, supershells, shell-like objects, and "worms". *Astrophys. J. Suppl.* **55,** 585-595 (1984).

5. Hartmann, D. & Burton, W. B. *Atlas of Galactic Neutral Hydrogen.* (Cambridge Univ. Press, Cambridge,1997).

6. Bally, J., Walawender, J., Johnstone, D., Kirk, H., Goodman, A. In *Handbook of Star Forming Regions* Vol. 1 (ed. Reipurth, B.) 308-345 (Astronomical Society of the Pacific, 2008).

7. HI4PI Collaboration, Ben Bekhti, N. Flöer, L. et al. HI4PI: A full-sky H I survey based on EBHIS and GASS. *Astron. Astrophys.* **594,** A116 (2016).

8. Dame, T. M., Hartmann, D. & Thaddeus, P. The Milky Way in molecular clouds: a new complete CO survey. *Astrophys. J.* **547,** 792-813 (2001).

9. Lim, T.-H., Min, K.-W., Seon, K.-I. Far-ultraviolet observations of the Taurus-Perseus-Auriga Complex. *Astrophys. J.* **765,** 107-117 (2013).

10. Heyer, M. H. & Dame, T. M. Molecular clouds in the Milky Way. *Annu. Rev. Astron. Astrophys.* **53,** 583-629 (2015).

11. Fukui, Y. & Kawamura, A. Molecular clouds in nearby galaxies. *Annu. Rev. Astron. Astrophys.* **48,** 547-580 (2010).

12. Dobbs C. L. et al. In *Protostars and Planets VI.* (ed. Beuther H., Klessen R. S., Dullemond C. P., Henning T.) 3-26 (Arizona Univ. Press, Tucson, 2014).

13. Ballesteros-Paredes, J. et al., From diffuse gas to dense molecular cloud cores. *Space Sci. Rev.* **216,** 16 (2020).

14. McCray, R. & Kafatos, M. Supershells and propagating star formation. *Astrophys. J.* **317,** 190-196 (1987).

15. Hartmann, L., Ballesteros-Paredes, J., Bergin, E. A. Rapid formation of molecular clouds and stars in the solar neighborhood. *Astrophys. J.* **562,** 852-868 (2001).

16. Inutsuka, S.-I., Inoue, T., Iwasaki, K., Hosokawa, T. The formation and destruction of molecular clouds and galactic star formation. An origin for the cloud mass function and star formation efficiency. *Astron. Astrophys.* **580,** A49 (2015).

17. Patel, N. A., Goldsmith, P. F., Heyer, M. H., Snell, R. L., Pratap, P. Origin and evolution of the Cepheus bubble. *Astrophys. J.* **507,** 241-253 (1998).

18. Fukui, Y. et al. Discovery of the Carina Flare with NANTEN; Evidence for a supershell that triggered the formation of stars and massive molecular clouds. *Pub. Astron. Soc. Jan.* **51,** 751-764 (1999).

19. Dawson, J. R. et al. Supershells as molecular cloud factories: Parsec resolution observations of H I and ^{12}CO (J = 1–0) in GSH 287+04-17 and GSH 277+00+36. *Astrophys. J.* **728,** 127 (2011).

20. Dawson, J. R. The supershell-molecular cloud connection: Large-scale stellar feedback and the formation of the molecular ISM. *Publ. Astron. Soc. Aust.* **30,** 25 (2013).

21. Ungerechts, H. & Thaddeus, P. A CO survey of the dark nebulae in Perseus, Taurus, and Auriga. *Astrophys. J. Suppl.* **63,** 645-660 (1987).

22. Zucker, C. et al. A large catalog of accurate distances to local molecular clouds: the Gaia DR2 edition. *Astrophys. J.* **879,** 125 (2019).

23. Azimlu, M., Martíenez-Galarza, J. R. Muench, A. A. A WISE census of young stellar objects in the Perseus OB2 association. *Astron. J.* **150,** 95 (2015).

24. Kruijssen, J. M. D. et al. Fast and inefficient star formation due to short-lived molecular clouds and rapid feedback. *Nature* **569**, 519-522 (2019).

25. Chevalier, R. A. The Evolution of supernova remnants. Spherically symmetric models. *Astrophys. J.* **188,** 501-516 (1974).

26. Tenorio-Tagle, G. & Bodenheimer, P. Large-scale expanding superstructures in galaxies. *Annu. Rev. Astron. Astrophys.* **26,** 145-197 (1988).

27. Castor, J., McCray, R., Weaver, R. Interstellar bubbles. *Astrophys. J.* **200,** L107-L110 (1975).

28. Yadav, N., Mukherjee, D., Sharma, P. Nath, B. B. How multiple supernovae overlap to form superbubbles. *Mon. Not. R. Astron. Soc.* **465,** 1720-1740 (2017).

29. Elmegreen, B. G. Star formation in a crossing time. *Astrophys. J.* **530,** 277-281(2000).

30. Wolk, S. J. et al. X-ray and infrared emission from young stellar objects near LkHα 101. *Astrophys. J.* **715,** 671-695 (2010).

31. Winkel et al. The Effelsberg-Bonn H I survey: Milky Way gas. First data release. *Astron. Astrophys.* **585,** A41 (2016).

32. Kalberla, P. M. W. & Haud, U. GASS: The Parkes Galactic all-sky survey. Update: improved correction for instrumental effects and new data release. *Astron. Astrophys.* **578,** A78 (2015).

33. Narayanan, G. et al. The Five College Radio Astronomy Observatory CO mapping survey of the Taurus molecular cloud. *Astrophys. J. Suppl.* **117,** 341-361 (2008).

34. Goldsmith, P. F. et al. Large-scale structure of the molecular gas in Taurus revealed by high linear dynamic range spectral line mapping. *Astrophys. J.* **680,** 428-445 (2008).

35. Ridge, N. A. et al. The COMPLETE survey of star-forming regions: Phase I data. *Astron. J.* **131,** 2921-2933 (2016).

36. Shan, W. et al. Development of superconducting spectroscopic array receiver: A multibeam 2SB SIS receiver for millimeter-wave radio astronomy. *IEEE Transactions on Terahertz Science and Technology* **2,** 593-604. (2012).

37. Sousbie, T. The persistent cosmic web and its filamentary structure - I. Theory and implementation. *Mon. Not. R. Astron. Soc.* **414,** 350-383 (2011).

38. Palmeirim, P. et al. Herschel view of the Taurus B211/3 filament and striations: evidence of filamentary growth? *Astron. Astrophys.* **550,** A38 (2013).

39. Shimajiri, Y. et al. Probing accretion of ambient cloud material into the Taurus B211/B213 filament. *Astron. Astrophys.* **623,** A16 (2019).

40. Wilson, T. L., Rohlfs, K., Hüttemeister, S. *Tools of Radio Astronomy* (Springer, Berlin, 2013).

41. Weaver, R., McCray, R., Castor, J., Shapiro, P., Moore, R. Interstellar bubbles. II - Structure and evolution. *Astrophys. J.* **218,** 377-395 (1977).

42. Kalberla, P. M. W. & Dedes, L. Global properties of the HI distribution in the outer Milky Way. Planar and extra-planar gas. *Astron. Astrophys.* **487,** 951-963 (2008).

43. Blaauw, A. On the origin of the O- and B-type stars with high velocities (the "run-away" stars), and some related problems. *Bull. Astron. Inst. Neth.* **15,** 265-290 (1961).

44. De Luca, A. et al. PSR J0357+3205: A fast-moving pulsar with a very unusual X-ray trail. *Astrophys. J. Lett.* **765,** L19 (2013).

45. Wright, N. J. OB Associations and their origins. *New Astronomy Reviews* **90,** 101549 (2020).

46. De Geus, E. J. Interactions of stars and interstellar matter in Scorpio Centaurus. *Astron. Astrophys.* **262,** 258-270 (1992).

47. Robitaille, J.-F. et al. Interstellar magnetic cannon targeting the Galactic halo. A young bubble at the origin of the Ophiuchus and Lupus molecular complexes. *Astron. Astrophys.* **617,** A101 (2018).

48. Krause, M. G. H. et al. Surround and squash: the impact of superbubbles on the interstellar medium in Scorpius-Centaurus OB2. *Astron. Astrophys.* **619,** A120 (2018).

49. Reynolds, R. J., & Ogden, P. M. Optical evidence for a very large, expanding shell associated with the I Orion OB association, Barnard's loop, and the high galactic latitude Hα filaments in Eridanus. *Astrophys. J.* **229,** 942-953 (1979).

50. Brown, A. G. A., Hartmann, D., Burton, W. B. The Orion OB1 association. II. The Orion-Eridanus bubble. *Astron. Astrophys.* **300,** 903-922 (1995).

51. Bally, J. In *Handbook of Star Forming Regions* Vol. 1 (ed. Reipurth, B.) 459-482 (Astronomical Society of the Pacific, 2008).

52. Ochsendorf, B. B., Brown, A. G. A., Bally, J., Tielens, A. G. G. M. Nested shells reveal the rejuvenation of the Orion-Eridanus superbubble. *Astrophys. J.* **808,** 111 (2015).

53. Pon, A. Kompaneets model fitting of the Orion-Eridanus superbubble. II. Thinking outside of Barnard's Loop. *Astrophys. J.* **827,** 42 (2016).

54. Sahu, M. S. A study of the ISM in Puppis-Vela including the GUM Nebula. Ph.D. Thesis. Kapteyn Institute, Postbus 800 9700 AV, Groningen, The Netherlands (1992).

55. Testori, J. C. et al. A radio continuum and neutral hydrogen counterpart to the IRAS Vela shell. *Astron. Astrophys.* **458,** 163-171 (2006).

56. Dame, T. M. et al. A composite CO survey of the entire Milky Way. *Astrophys. J.* **322,** 706-720 (1987).

57. Murphy, D. C. & May, J. Molecular clouds in Vela. *Astron. Astrophys.* **247,** 202-214 (1991).

58. Yamaguchi, N. et al. Distribution and kinematics of the molecular clouds in the Gum Nebula. *Pub. Astron. Soc. Jan.* **51,** 765-774 (1999).

59. Case, W. et al. The X-ray superbubble in Cygnus. *Astrophys. J.* **238,** L71-L76 (1980).

60. Bochkarev, N. G. & Sitnik, T. G. Structure and origin of the Cygnus superbubble. *Astrophysics and Space Science* **108,** 237-302 (1985).

61. Kimura, M. et al. Is the Cygnus superbubble a hypernova remnant? *Pub. Astron. Soc. Jan.* **65,** 14 (2013).

62. Uyanıker, B., Fürst, E., Reich, W., Aschenbach, B., Wielebinski, R. The Cygnus superbubble revisited. *Astron. Astrophys.* **371,** 675-697 (2001).

63. Ábrahám, P., Balázs, L. G., Kun, M. Morphology and kinematics of the Cepheus Bubble. *Astron. Astrophys.* **354,** 645-656 (2000).

64. Dawson, J. R., Mizuno, N., Onishi, T., McClure-Griffiths, N. M., Fukui, Y. The 'Carina Flare' supershell: probing the atomic and molecular ISM in a Galactic chimney. *Mon. Not. R. Astron. Soc.* **387,** 31-44 (2008).

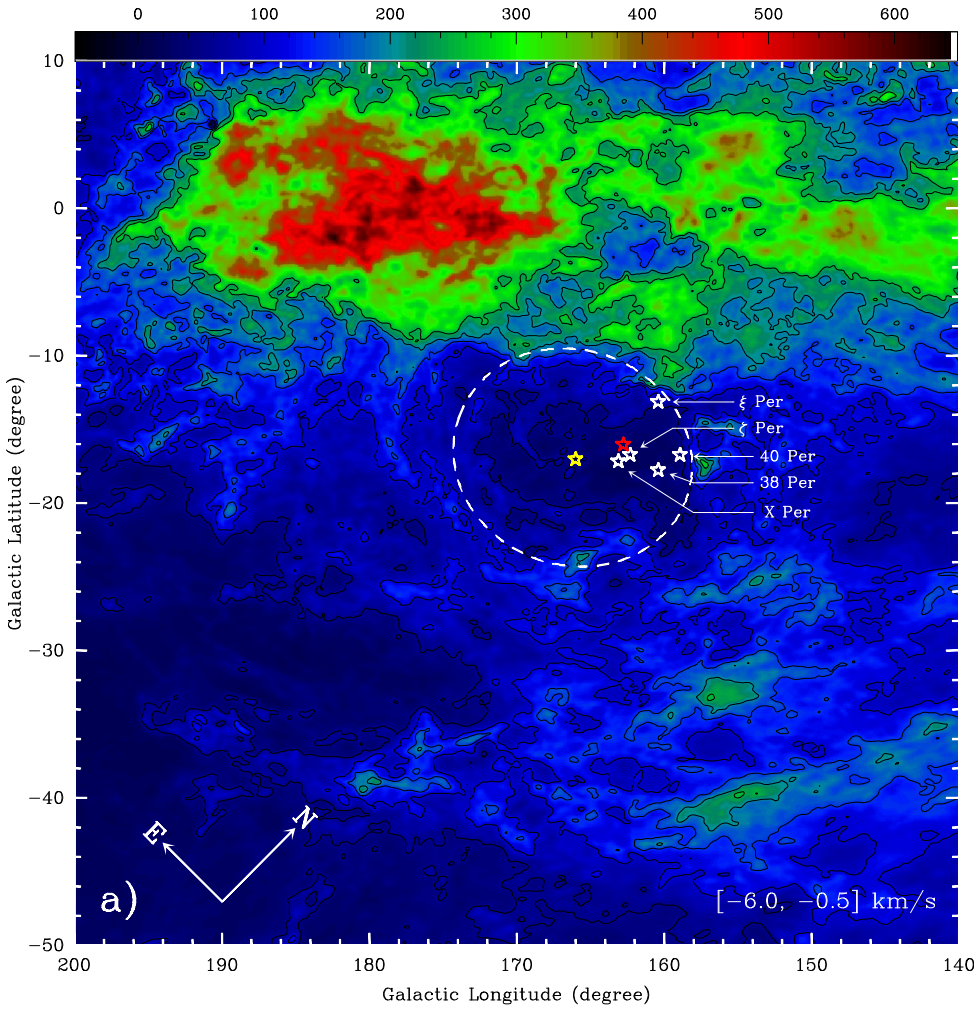
0
100
200
300
400
500
600
10
0
−10
−20
−30
−40
−50
200
190
180
170
160
150
140
Galactic Latitude (degree)
Galactic Longitude (degree)
ξ Per
ζ Per
40 Per
38 Per
X Per
E
N
a)
[−6.0, −0.5] km/s

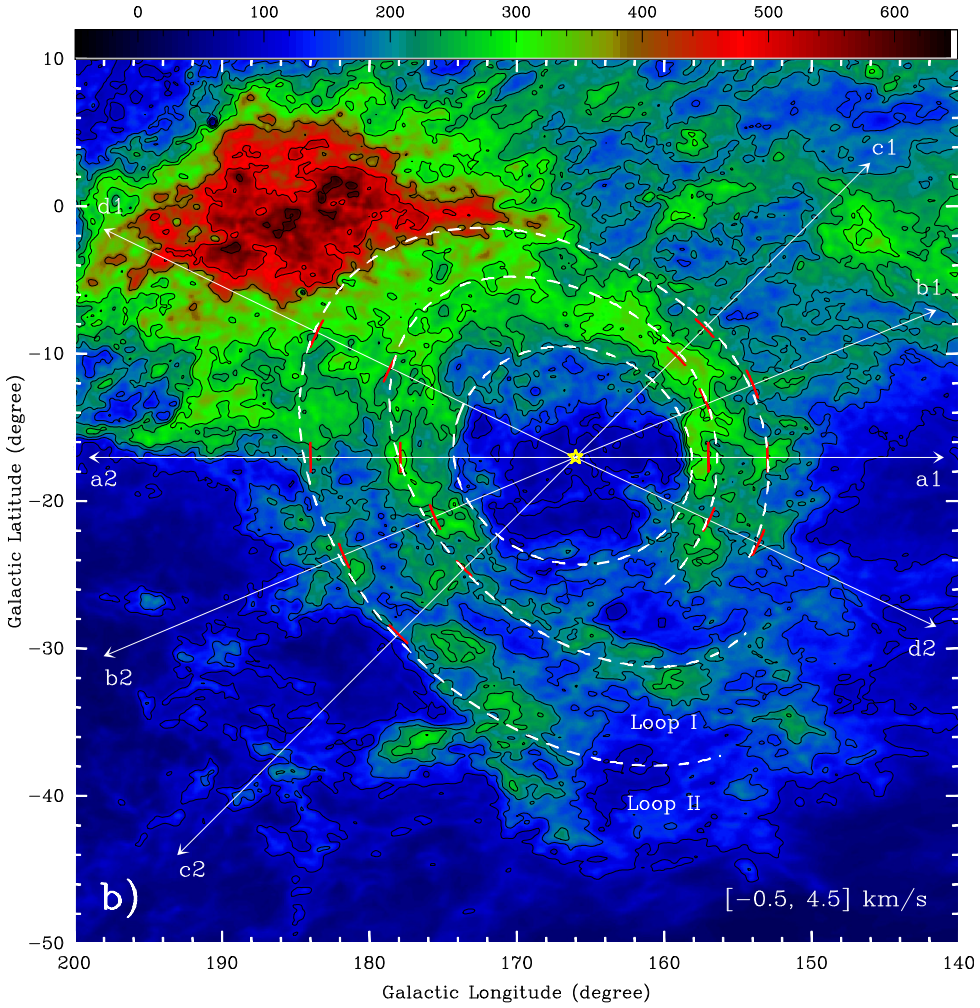
0
100
200
300
400
500
600
10
0
−10
−20
−30
−40
−50
Galactic Latitude (degree)
200
190
180
170
160
150
140
Galactic Longitude (degree)
a1
a2
b1
b2
c1
c2
d1
d2
Loop I
Loop II
b)
[−0.5, 4.5] km/s

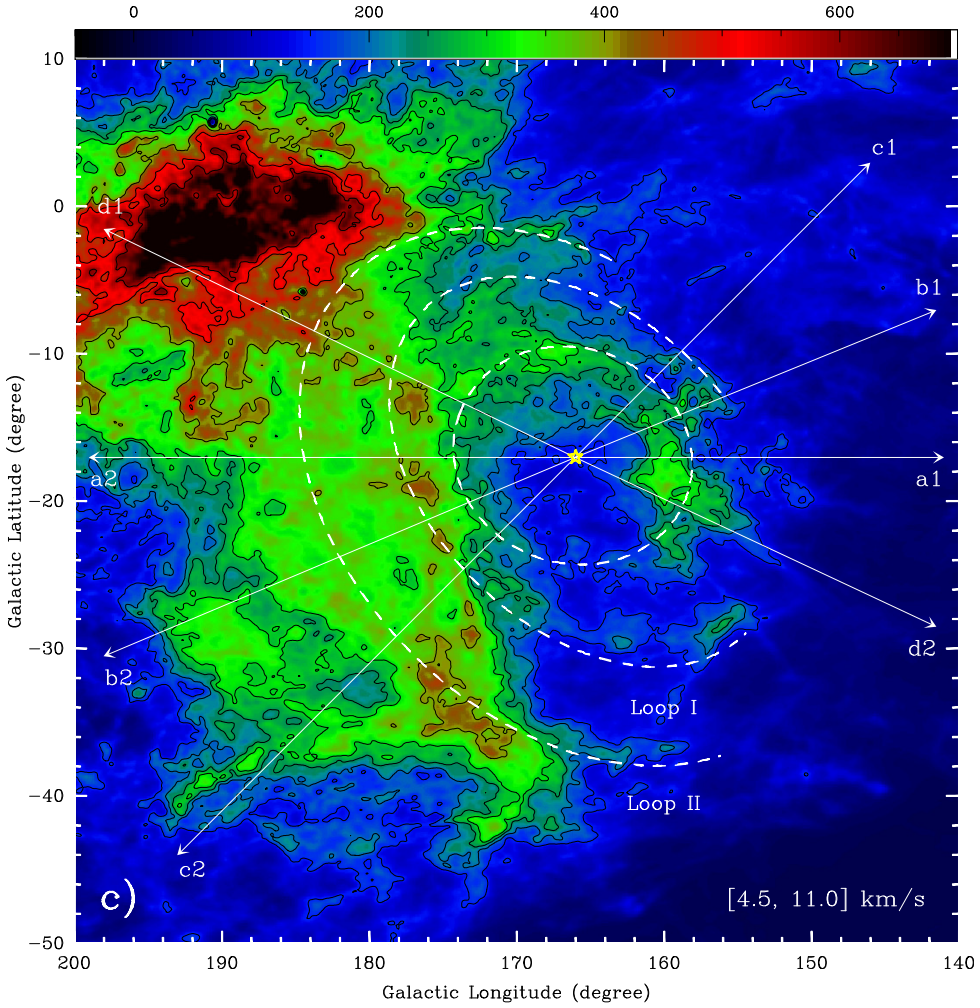
0
200
400
600
10
0
−10
−20
−30
−40
−50
200
190
180
170
160
150
140
Galactic Latitude (degree)
Galactic Longitude (degree)
c1
d1
b1
a2
a1
d2
b2
Loop I
Loop II
c2
c)
[4.5, 11.0] km/s

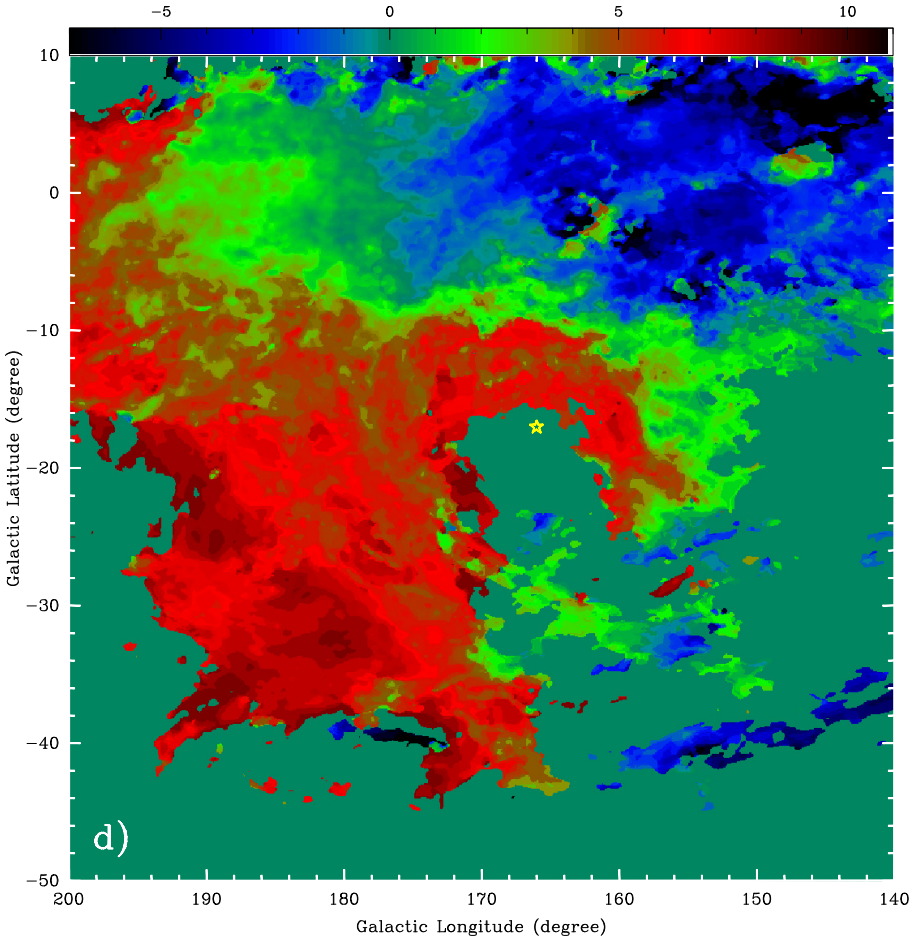

Figure 1 | Wide-field HI4PI HI images toward Per OB2. a, The intensity image integrated within the velocity range of [–6.0, –0.5]. The unit of the scale bar is K km s^{-1}. The contours correspond to 50, 100, 150, 200, and 250 K km s^{-1}. White stellar symbols show the positions of massive OB stars in Per OB2 (refs.[1,2]), while red stellar symbol shows the position of pulsar PSR J0357+3205 (see Methods). The white ellipse shows the cavity opened by Per OB2, which was also seen in previous observations (refs.[3,5]). **b,** Similar to panel a, but integrated within the velocity range of [–0.5, +4.5] km s^{-1}. The contours start from 150 K km s^{-1} and then increase by steps of 50 K km s^{-1}. The white arrow lines show the PV routings across the superbubble (see Figure 2). The red short lines show the positions of the loops detected in both the intensity images and PV diagrams (see Figure 2), while the white open ellipses show the fittings toward HI Loops I and II. **c,** Similar to panel b, but integrated within the velocity range of [+4.5, +11.0] km s^{-1}. **d,** The velocity field (1st moment), integrated between –6 and +11 km s^{-1}. The unit of the scale bar is km s^{-1}. For all panels, yellow stellar symbol marks the position of l = 166.0°, b = –17.0°.

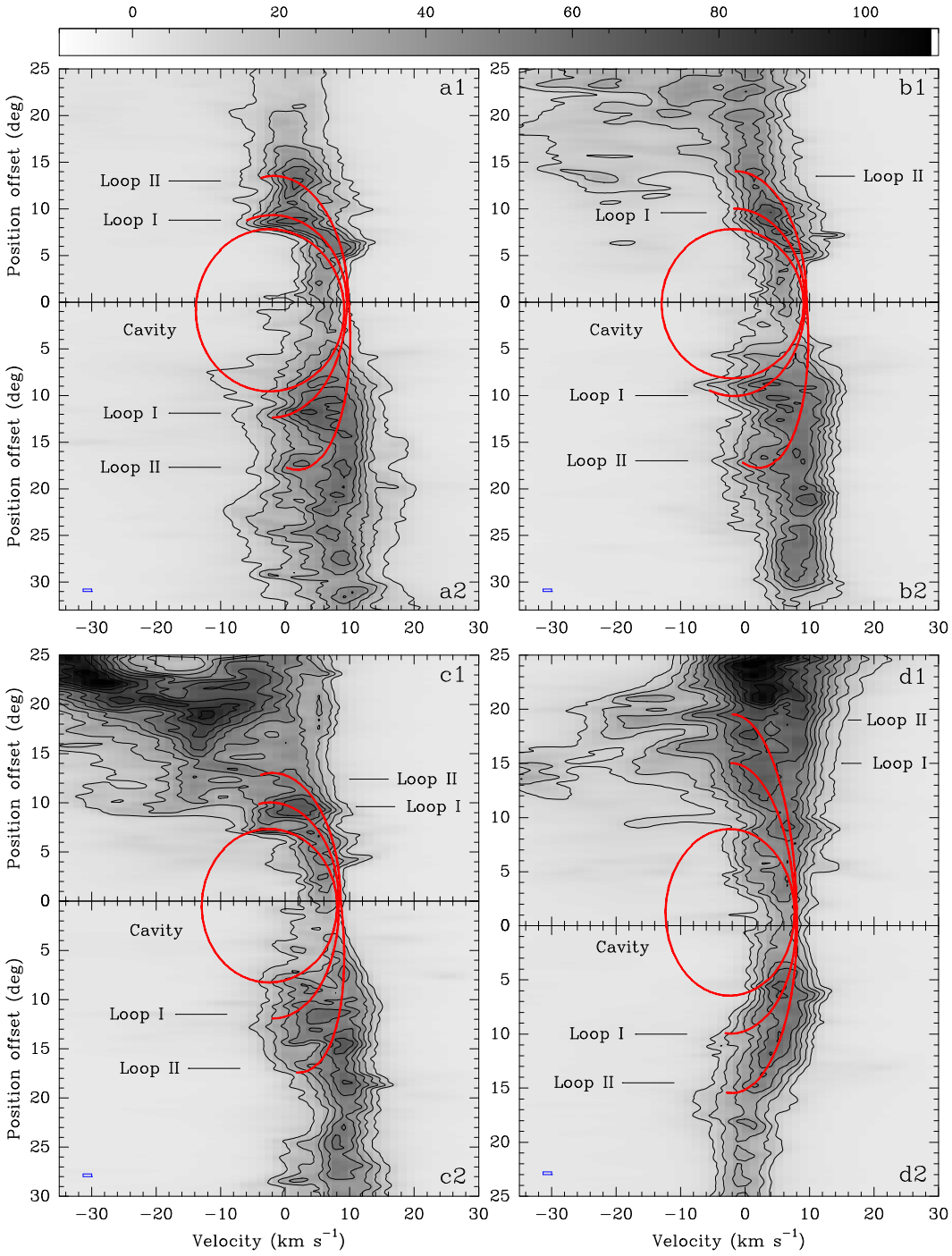

Figure 2 | The HI PV diagrams across the Per OB2 superbubble. The unit of the scale bar is K. The contours start from 15 K and increase in steps of 10 K in the directions of c1/c2, and start from 10 K and increase in steps of 10 K in rest directions. For all the panels, red ellipses show the fittings toward the central cavity, and HI loops I and II. The blue rectangle shows the resolutions in the HI4PI observations (16.2′ and 1.3 km s^{-1}).

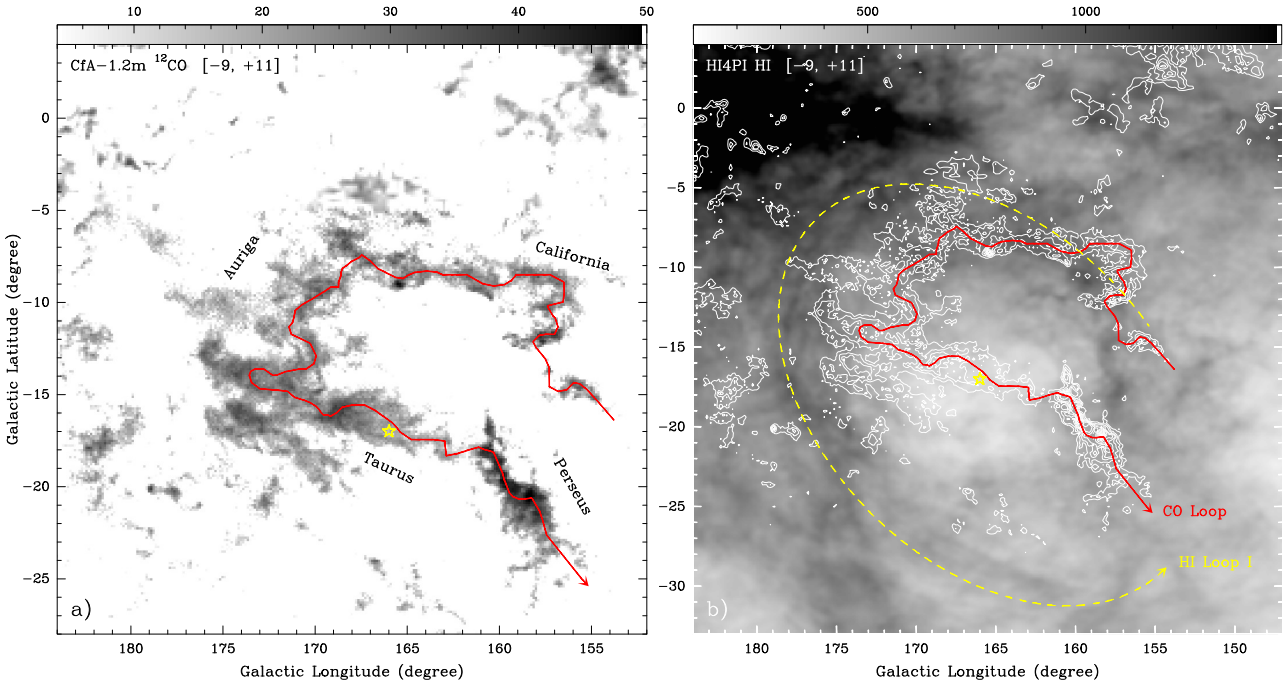

Figure 3 | Wide-field CfA 1.2 m CO intensity images toward Per OB2. a, The CO intensity image (grey scale), integrated within [–9, 11] km s^{-1}. Red line shows the ridge of the Taurus-Auriga-California-Perseus cloud loop (see Methods). **b,** The contours of CO intensity image (white), plotted on the HI4PI HI intensity image (grey scale) integrated within the same velocity range. The CO contours start from 6 K km s^{-1} and increase in steps of 6 K km s^{-1} ($1\,\sigma \sim 0.6$-1.0 K km s^{-1}). The unit of scale bar for the two panels is K km s^{-1}.

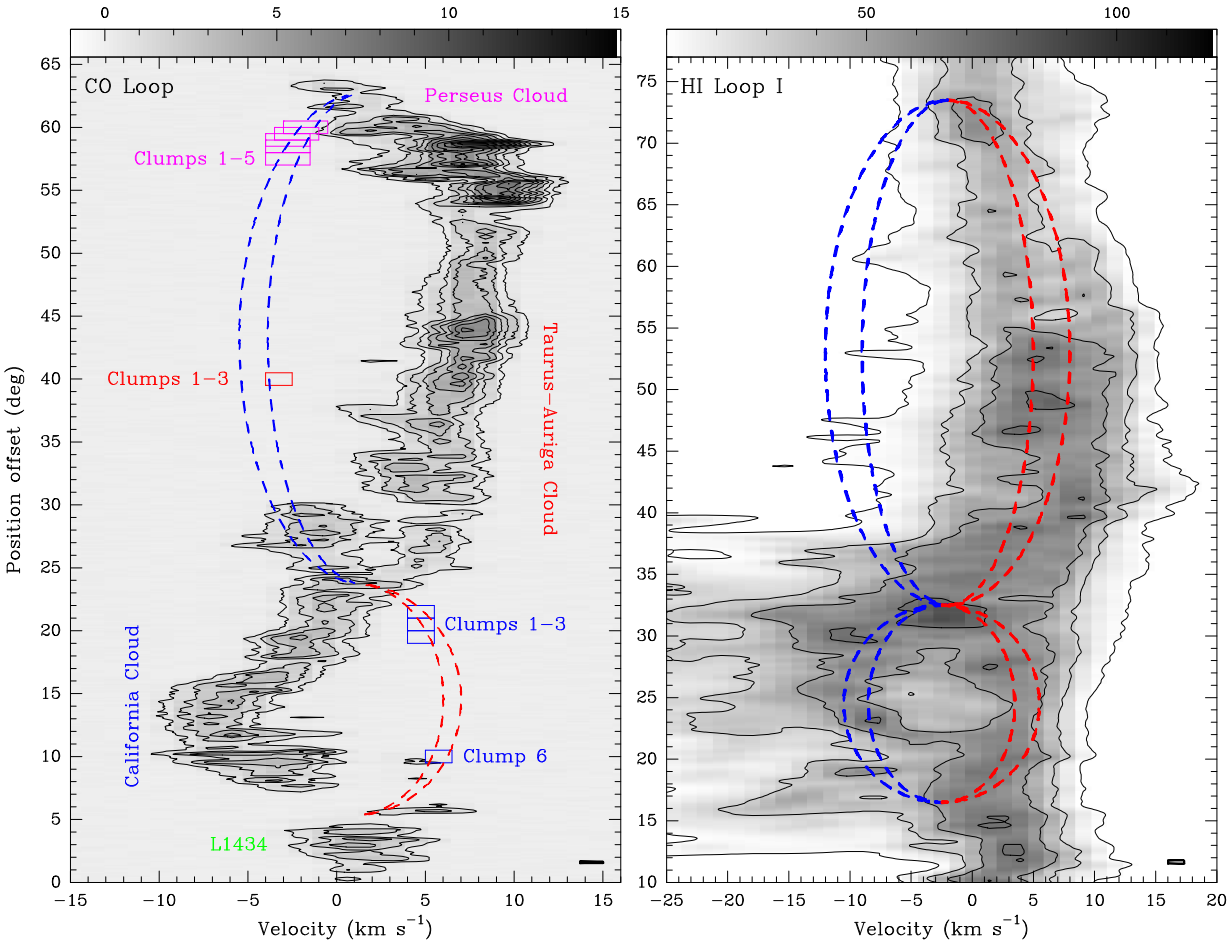

Figure 4 | The PV diagrams along the CO loop (left) and HI Loop I (right). The PV diagram of CO loop (grey scale and contours) is produced from the CfA 1.2 m CO data along the routing shown in Figure 3a. The contours start from 0.6 K and then increase by steps of 1.0 K. Different color rectangles show the clumps found in the complementary images from the FCRAO 14 m and PMO 13.7 m CO observations toward the Taurus, California, and Perseus Clouds, respectively (see Methods and Supplementary Figure 4). Blue and red dashed ellipses show the fittings toward these clumps. For the HI Loop I, contours start from 10 K and then increase by steps of 20 K. Blue and red dashed ellipses show the fittings toward the HI data.

Correspondence and Requests for Materials should be addressed to Xuepeng Chen (xpchen@pmo.ac.cn).

Acknowledgements This work is based on data products from the HI4PI HI, CfA 1.2 m and FCRAO 14 m CO surveys. We are grateful to the staff of Qinghai Radio Station of PMO at Delingha for the support during the CO observations.

Author Contributions X.C. leaded the studying of the Per OB2 superbubble and drafted the manuscript. W.G. and J.F. helped to reduce the HI and CO line data. All authors contributed to the data analysis and commented on the manuscript.

Competing interests The authors declare no competing financial interests.

The Perseus OB2 Superbubble and the Taurus-Auriga-California-Perseus Molecular Cloud Loop

Xuepeng Chen[1,2*], Weihua Guo[1,2], Jiancheng Feng[1,2], Yang Su[1], Yan Sun[1], Qingzeng Yan[1], Min Fang[1], and Ji Yang[1,2]

[1]*Purple Mountain Observatory & Key Laboratory of Radio Astronomy, Chinese Academy of Sciences, 10 Yuanhua Road, 210023 Nanjing, China*

[2]*School of Astronomy and Space Science, University of Science and Technology of China, Hefei, Anhui 230026, China*

Supplementary Materials

Supplementary Figure 1: The velocity channel maps of the HI4PI HI emission.

Supplementary Figure 2: The velocity channel maps of the CfA 1.2 m CO emission.

Supplementary Figure 3: The CfA 1.2 m CO intensity images, plotted on the HI4PI HI intensity images.

Supplementary Figure 4: The CfA 1.2 m CO image toward the molecular cloud loop, and complementary FCRAO 14 m and PMO 13.7 m CO images.

Supplementary Figure 5: The CO velocity fields of the Taurus-Auriga-California-Perseus Clouds.

Supplementary Table 1: Basic parameters of well-studied superbubbles in the solar vicinity.

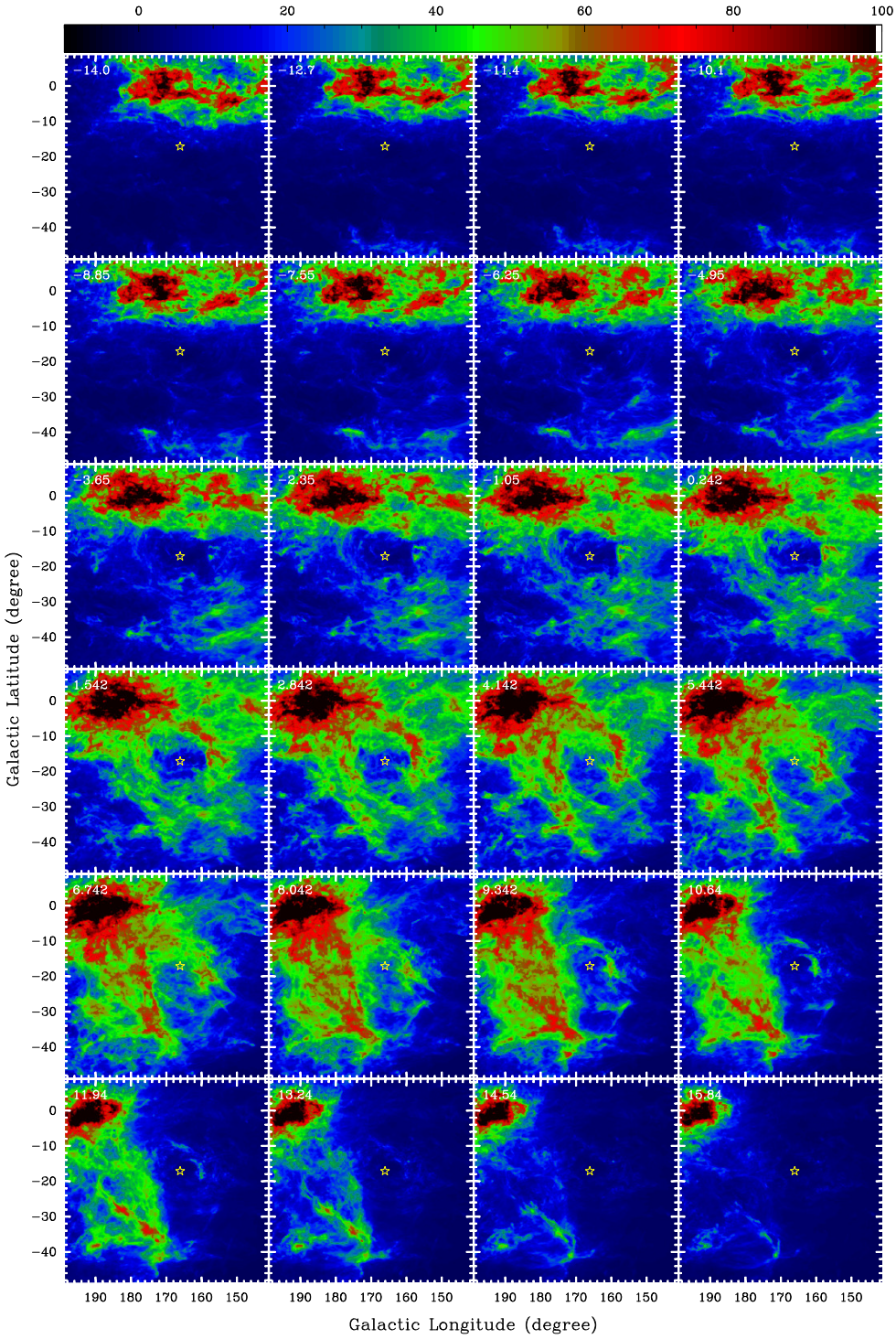

Supplementary Figure 1 | The velocity channel maps of the HI4PI HI emission. The unit of the scale bar is K. The channel velocity is written in the top left corner of each panel (in km s^{-1}). For all panels, yellow stellar symbol marks the position of $l = 166.0°$, $b = -17.0°$.

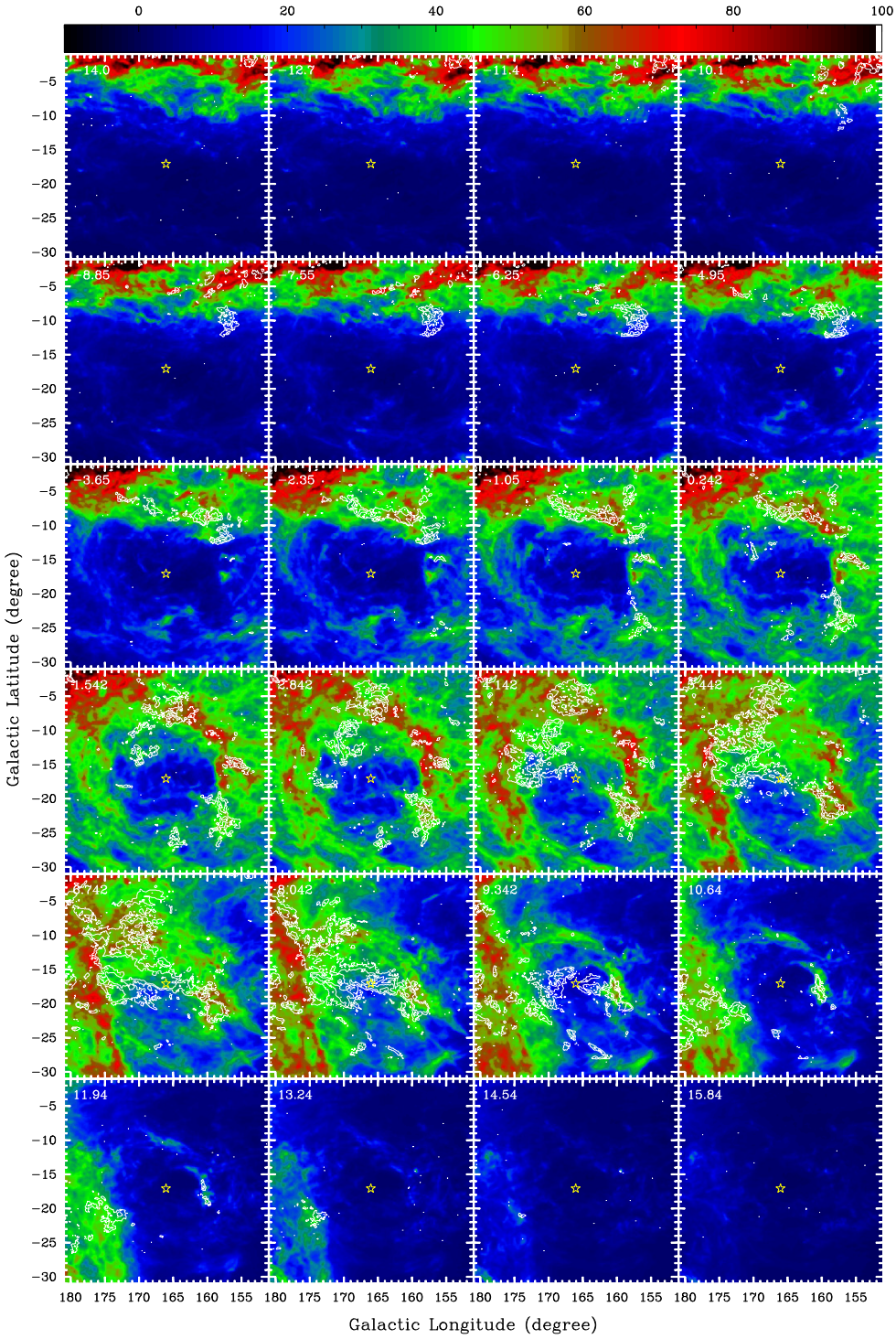

Supplementary Figure 2 | The velocity channel maps of the CfA 1.2 m CO emission (contours), plotted on the HI4PI HI images. The unit of the scale bar is K. In each panel, CO contour levels correspond to 0.6 and 2.4 K, where 1 σ level is $\sim$0.15 K.

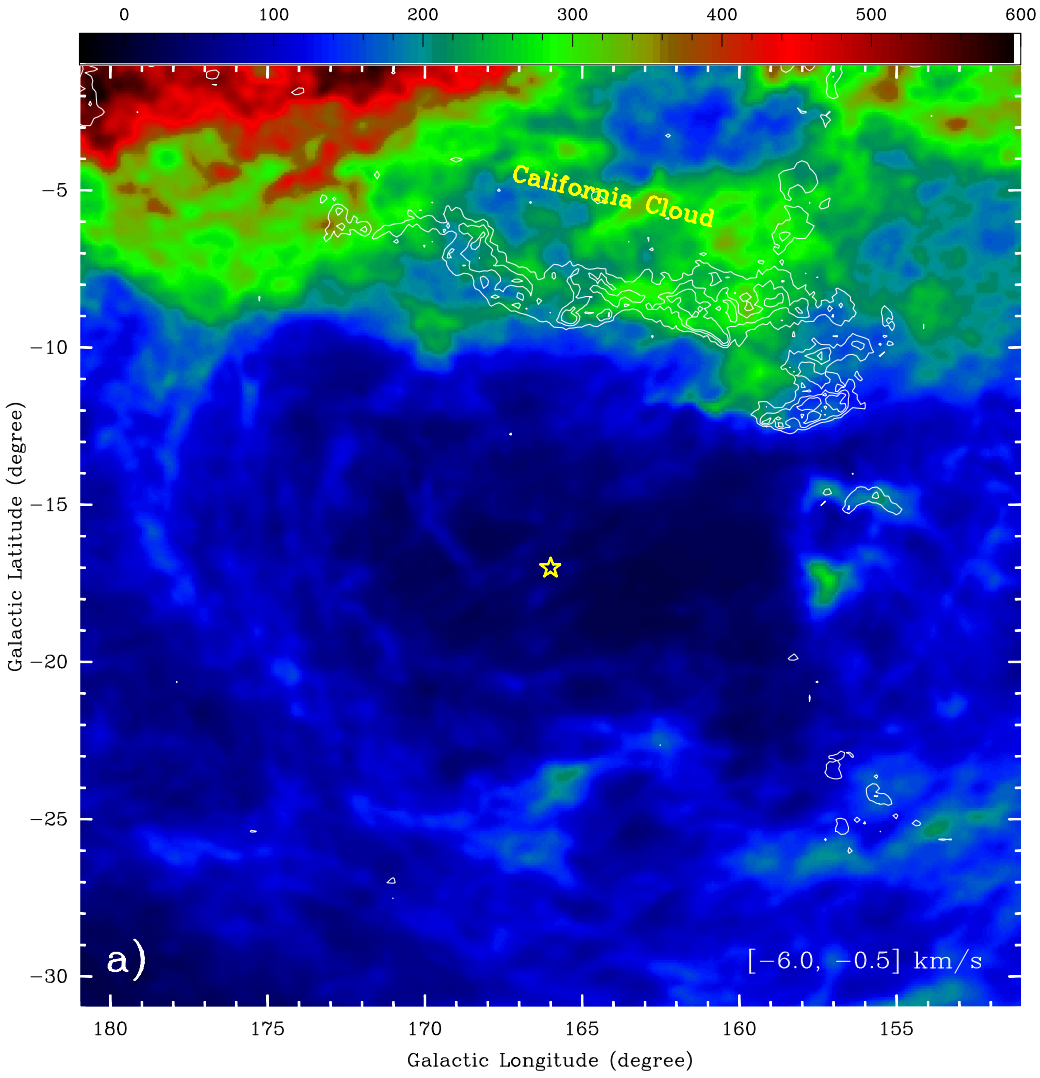
0
100
200
300
400
500
600
California Cloud
−5
−10
−15
−20
−25
−30
Galactic Latitude (degree)
a)
[−6.0, −0.5] km/s
180
175
170
165
160
155
Galactic Longitude (degree)

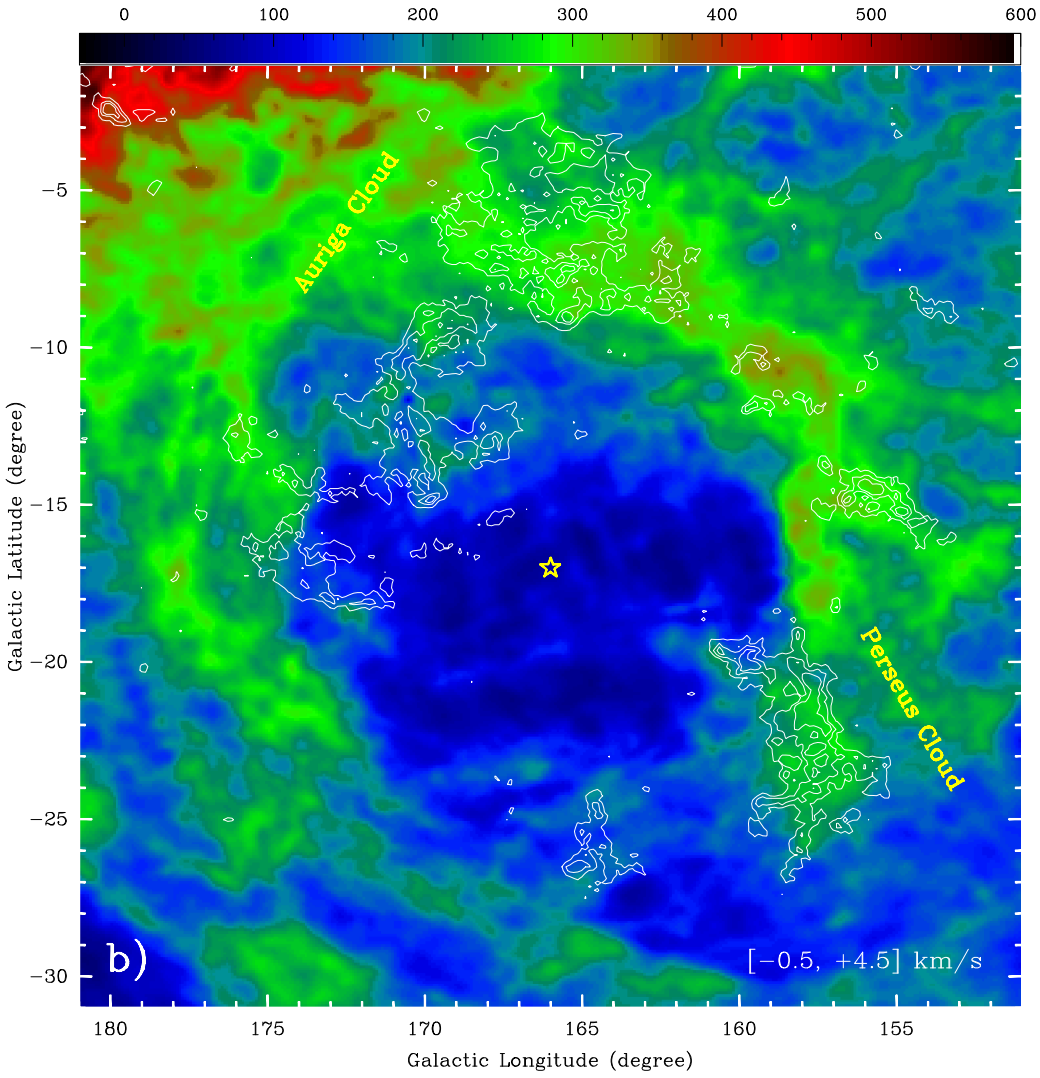
0
100
200
300
400
500
600
Auriga Cloud
Perseus Cloud
b)
[−0.5, +4.5] km/s
−5
−10
−15
−20
−25
−30
Galactic Latitude (degree)
180
175
170
165
160
155
Galactic Longitude (degree)

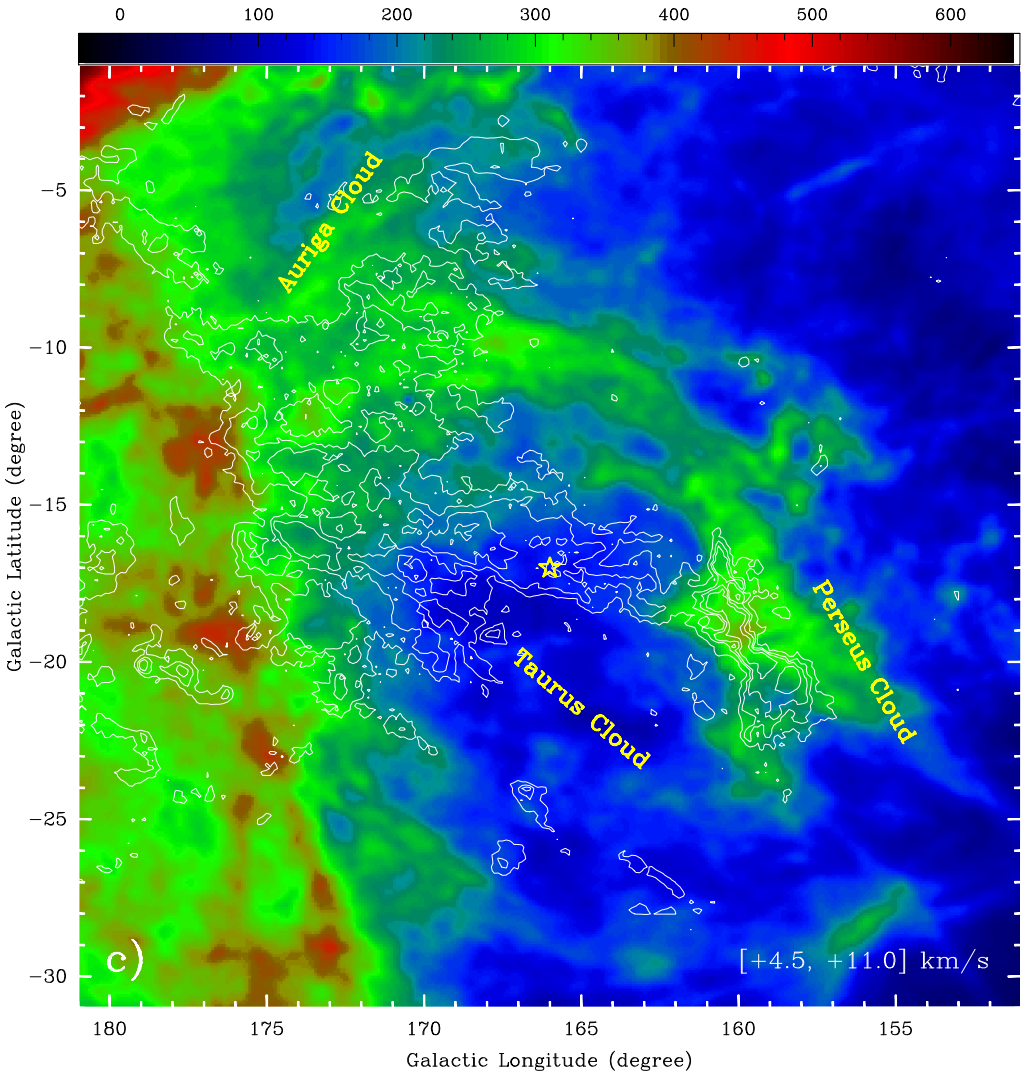

Supplementary Figure 3 | The CfA 1.2 m CO intensity images (white contours), plotted on the HI4PI HI intensity images. a, The intensity image integrated within the velocity range of [–6.0, –0.5]. The unit of the scale bar is K km s^{-1}. The CO contours correspond to 5, 15, and 25 σ (1 $\sigma \sim$ 0.45 K km s^{-1}). **b,** Similar to panel a, but integrated within the velocity range of [–0.5, +4.5] km s^{-1}. The CO contours correspond to 5, 15, and 25 σ (1 $\sigma \sim$ 0.48 K km s^{-1}). **c,** Similar to panel a, but integrated within the velocity range of [+4.5, +11.0] km s^{-1}. The CO contours correspond to 5, 15, 25 and 45 σ (1 $\sigma \sim$ 0.55 K km s^{-1}).

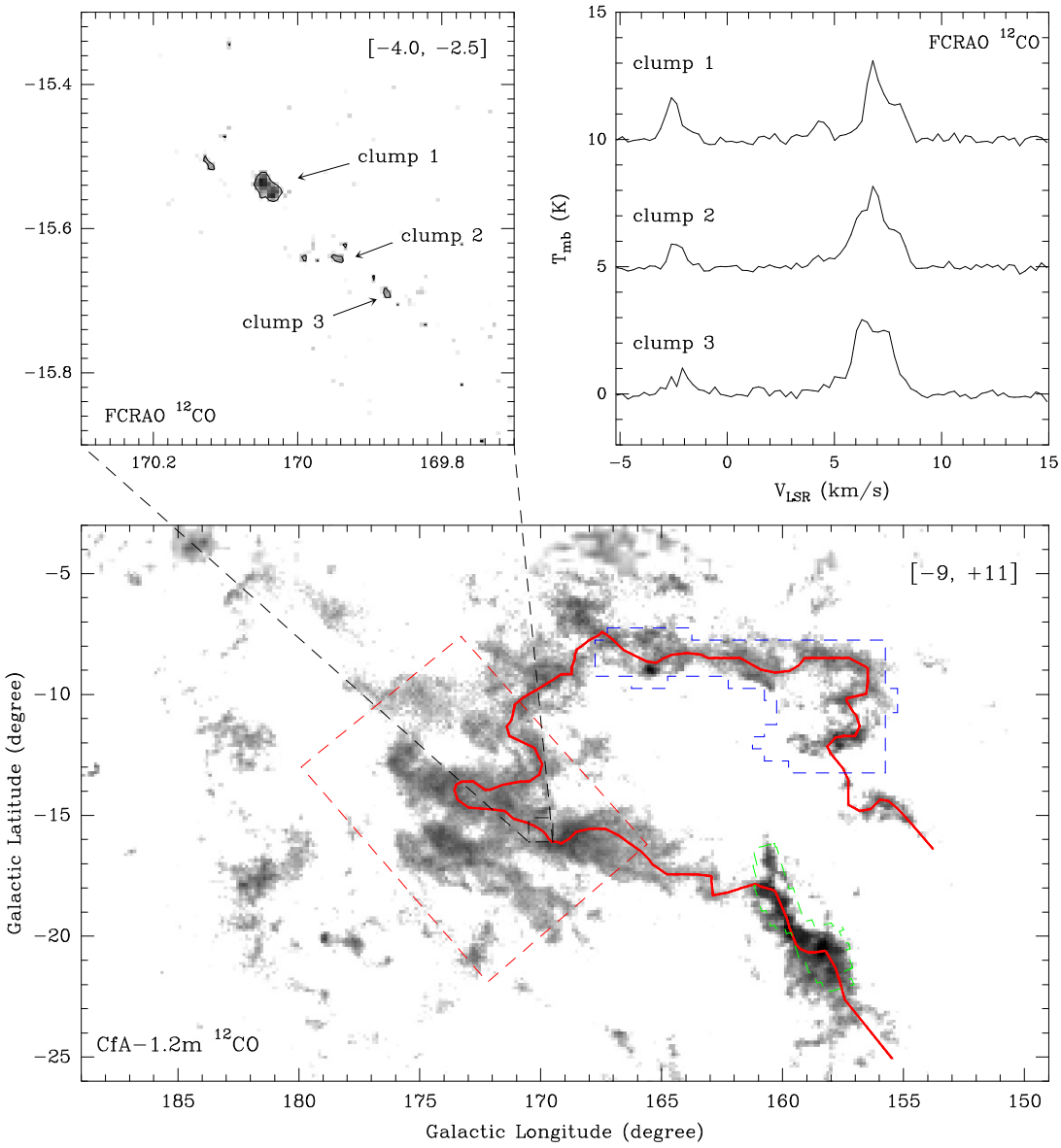

Supplementary Figure 4a | The CfA 1.2 m CO image toward the molecular cloud loop, and complementary FCRAO 14 m ^{12}CO images toward the Taurus Cloud. The red line in the CfA 1.2 m CO image shows the ridge along the Taurus-Auriga-California-Perseus cloud loop. The top left panel shows the FCRAO 14 m CO intensity image toward the central Taurus region integrated within [–4.0, –2.5] km s^{-1}, and the contour corresponds to 4 σ (1 σ $\sim$ 0.125 K km s^{-1}). The top right panel shows the CO spectra for the clumps found in Taurus.

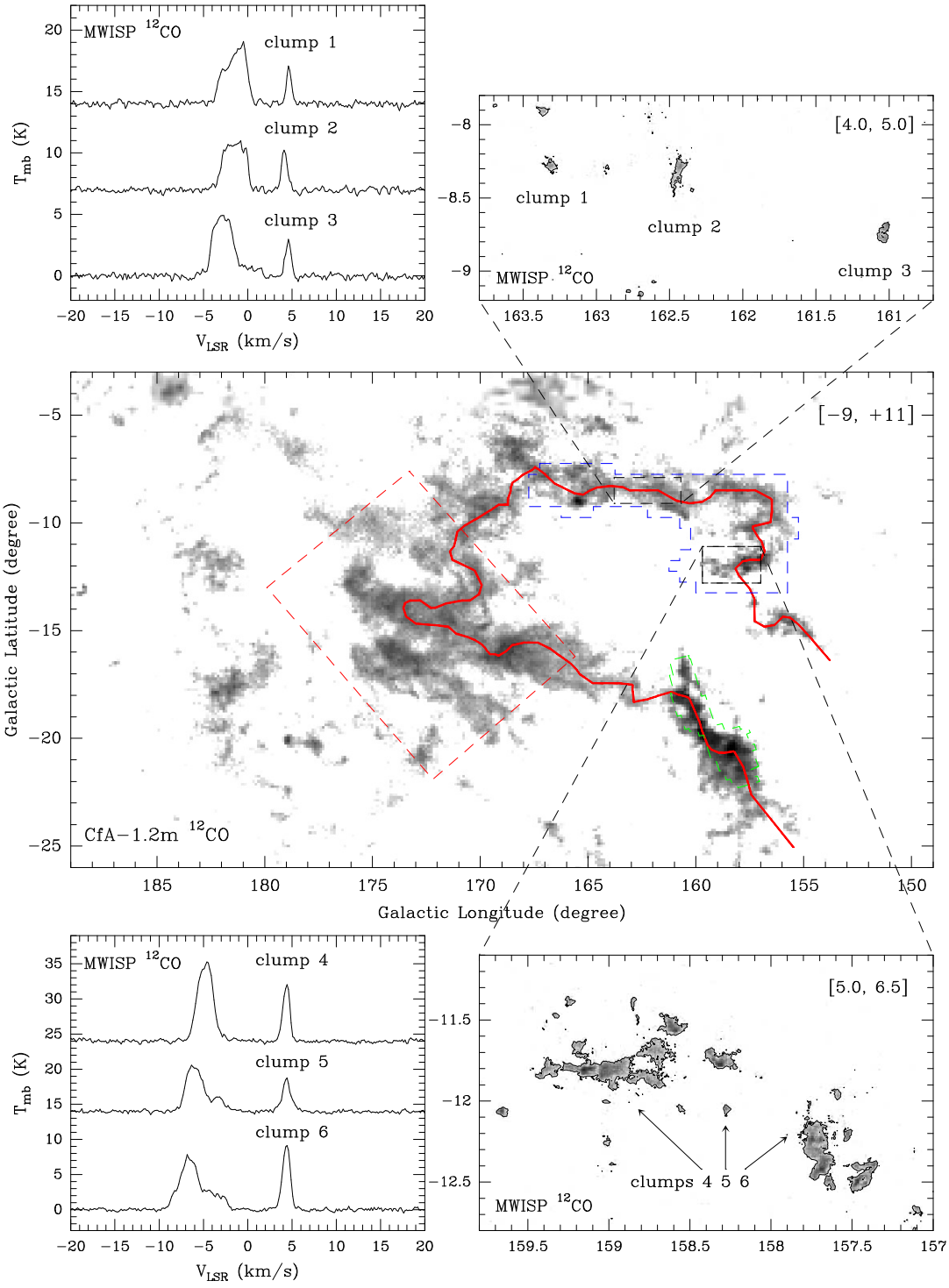

Supplementary Figure 4b | The complementary MWISP ^{12} CO images toward the California Cloud. The MWISP CO intensity images are integrated within [4.0, 5.0] km s^{-1} (top right) and [5.0, 6.5] km s^{-1} (bottom right). The contour corresponds to 4 σ, where 1 σ is 0.25 (top right) and 0.35 K km s^{-1} (bottom right), respectively.

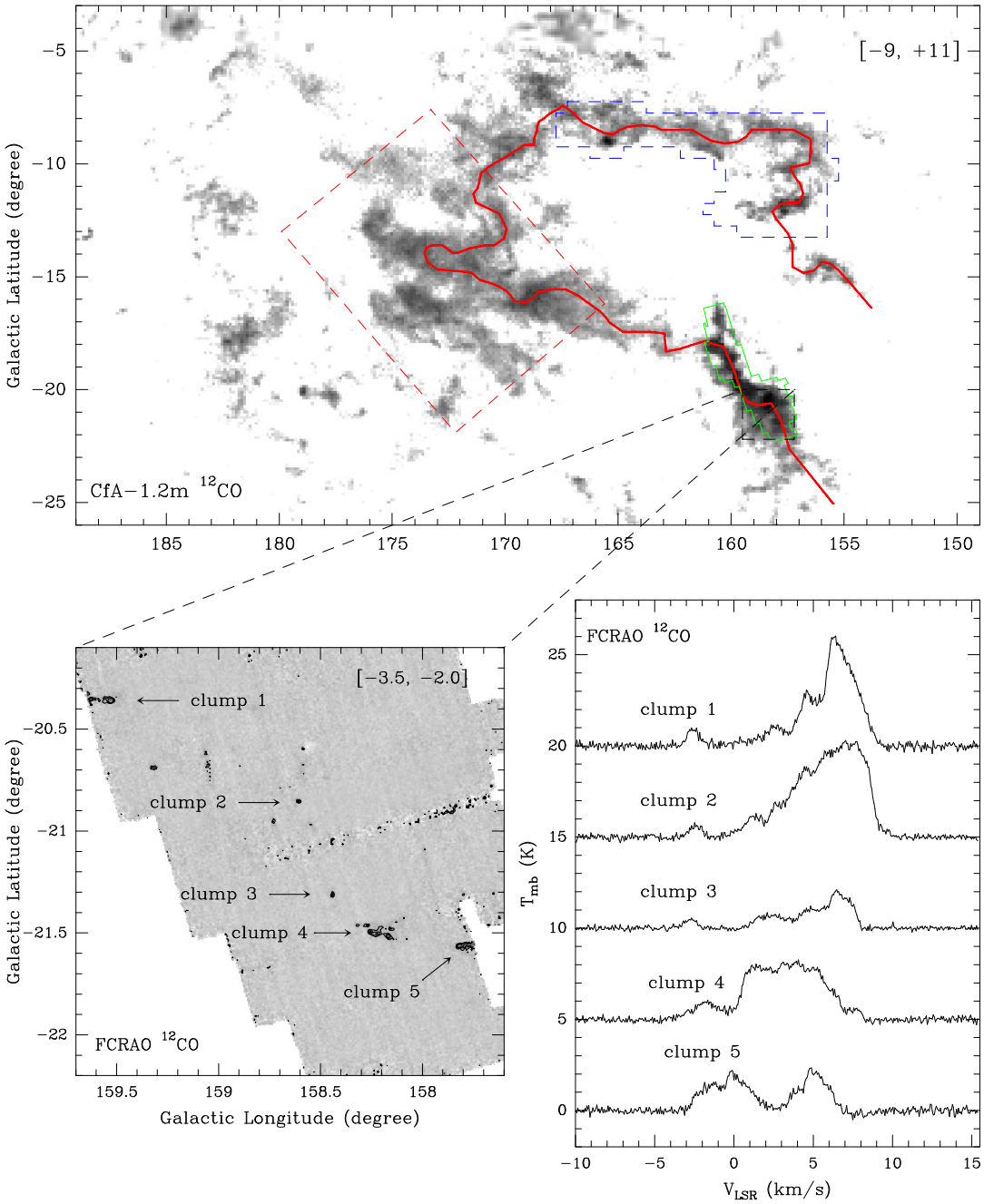

Supplementary Figure 4c | The complementary FCRAO 14 m ^{12}CO images toward the Perseus Cloud. The FCRAO CO image is integrated within [–3.5, –2.0] km s^{-1}, and the contours correspond to 5, 7, and 9 σ (1 $\sigma \sim$ 0.08 K km s^{-1}).

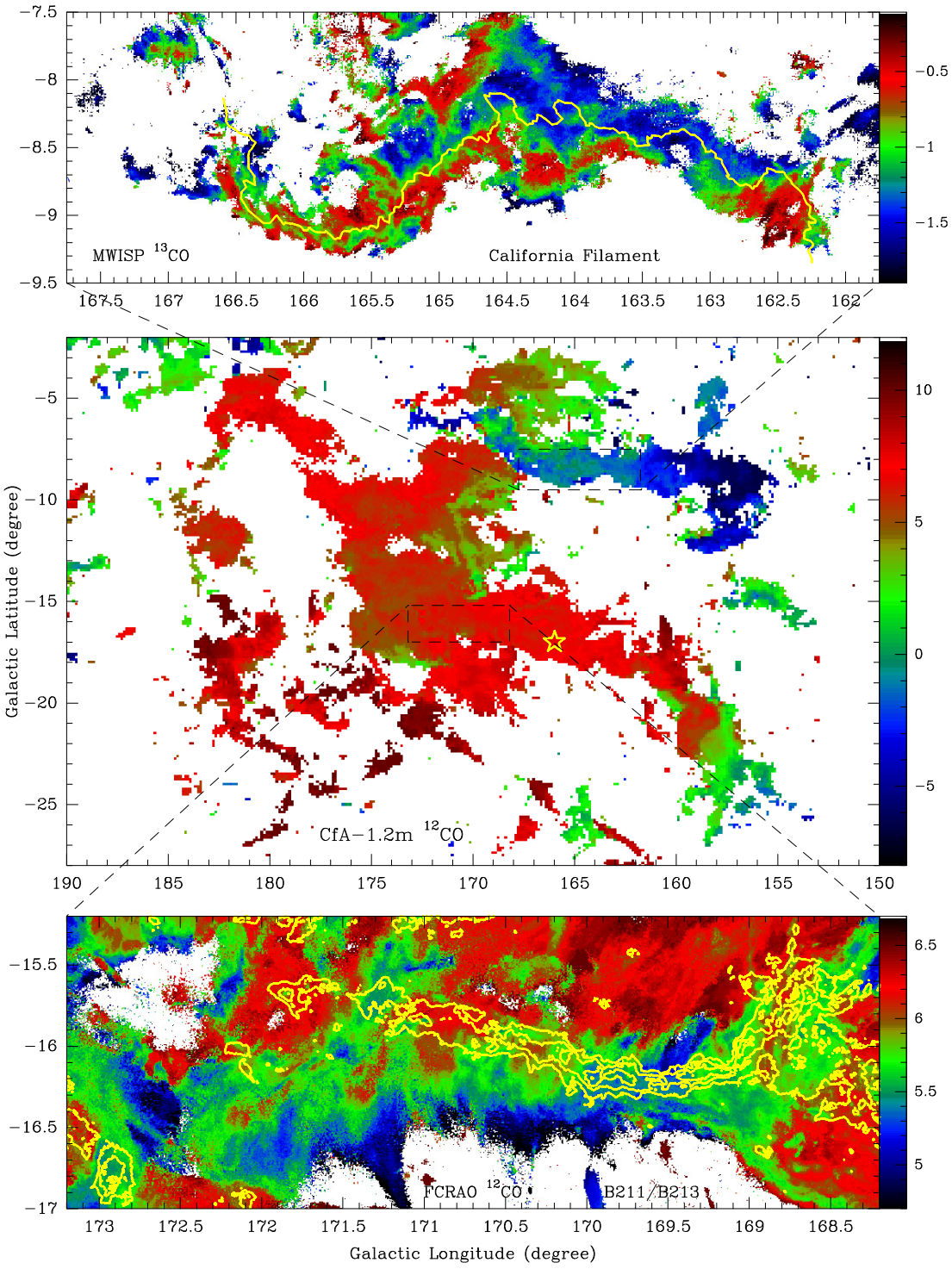

Supplementary Figure 5 | The CO velocity fields of the Taurus-Auriga-California-Perseus Clouds. The middle panel shows the CfA 1.2 m ^{12}CO velocity field, integrated within [–7, +10] km s^{-1}. The bottom panel shows the

FCRAO 14 m ^{12}CO velocity field (integrated within [4.5, 6.5] km s^{-1}) toward the B211/B213 filamentary structure, overlapped with the ^{13}CO contours. The contours start from 1.5 K km s^{-1} and then increase in steps of 1 K km s^{-1}. The top panel shows the MWISP ^{13}CO velocity field (integrated within [–2.0, 0.0] km s^{-1}) toward the filamentary structure (yellow line) identified in the California Cloud (Guo et al. in prep.).

Table 1. Basic parameters of well-studied superbubbles in the solar vicinity.

Superbubble Name	Distance (pc)	Diameter (pc)	Kinetic Age (Myr)	HI Gas Morphology	Molecular Clouds Morphology	References
Upper Sco	145	~ 65	~ 3	Loop	Filament	refs.[47,48]
Per OB2	300	~ 330	~ 10	Shell/Loop	Loop	This work
Orion-Eridanus	400	140×300	$\sim$ 5-10	Shell/Loop	Filament	refs.[51,52]
IRAS Vela Shell	450	~ 120	~ 5	Shell	Ridge	refs.[55,58]
Cepheus	900	~ 120	~ 7	Shell	Ring	refs.[17,63]
Carina Flare	2600	230×360	~ 10	Shell	Ring	refs.[18,64]

Figures

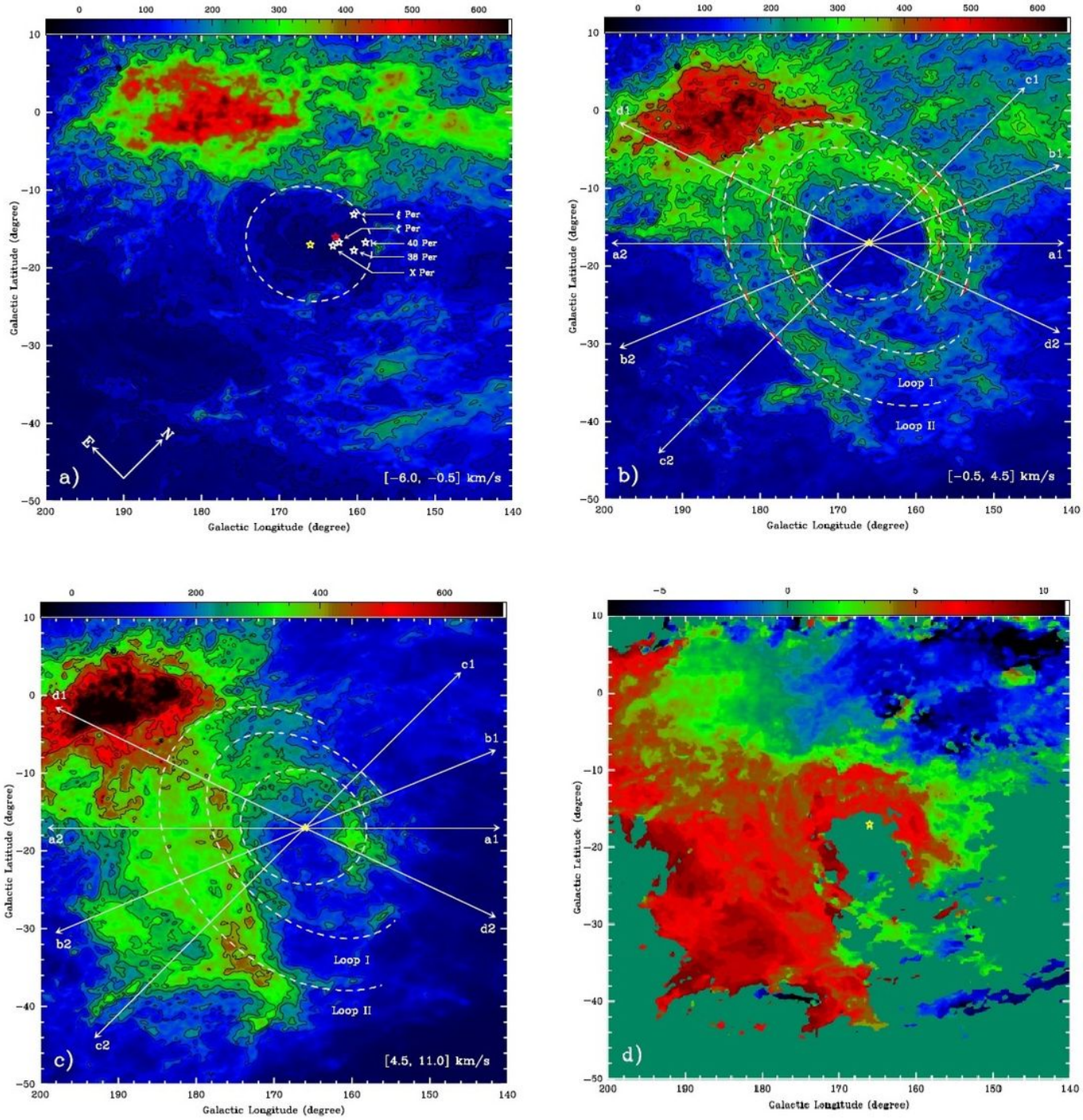

Figure 1

Wide-field HI4PI HI images toward Per OB2. (see Manuscript file for full figure legend)

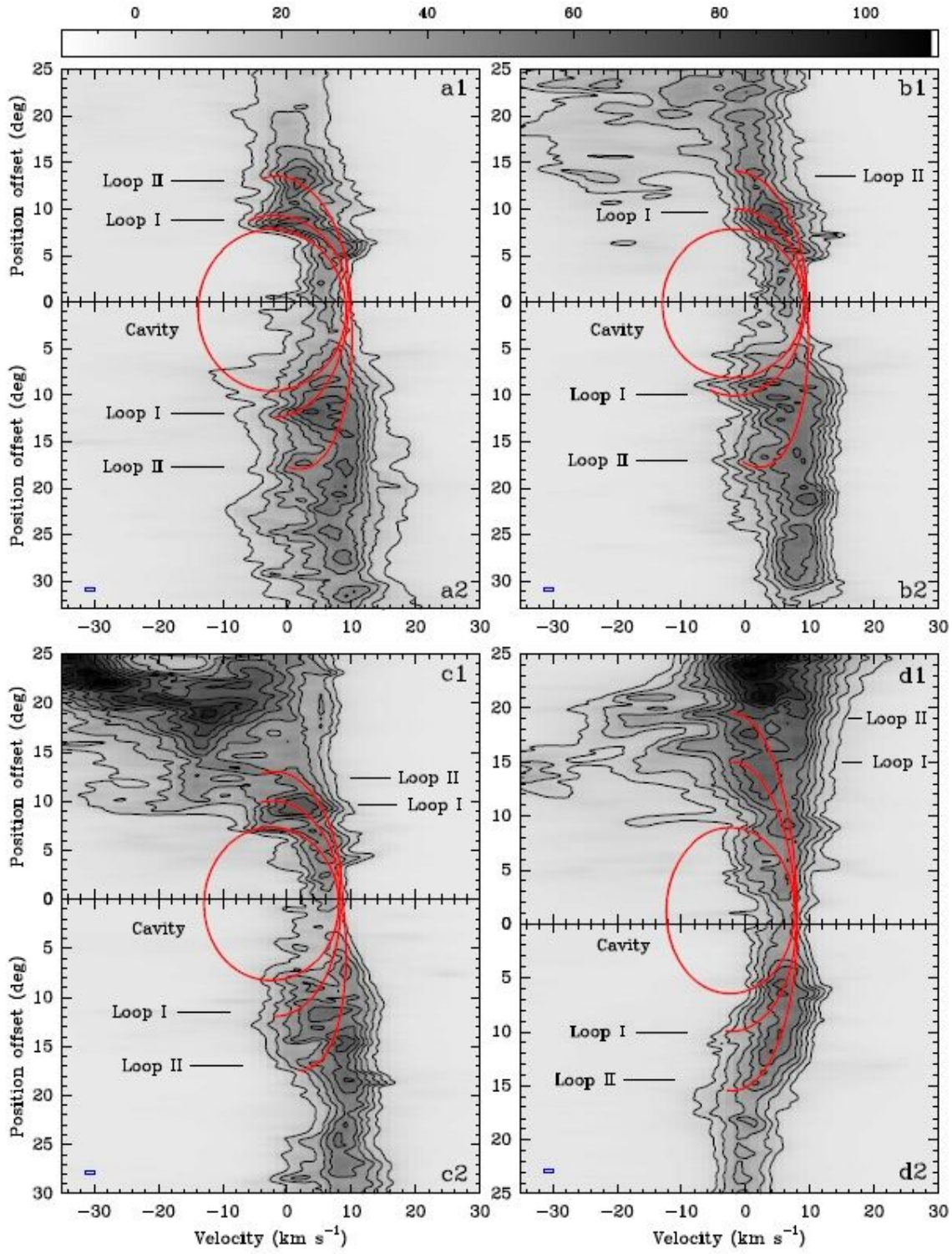

Figure 2

The HI PV diagrams across the Per OB2 superbubble. (see Manuscript file for full figure legend)

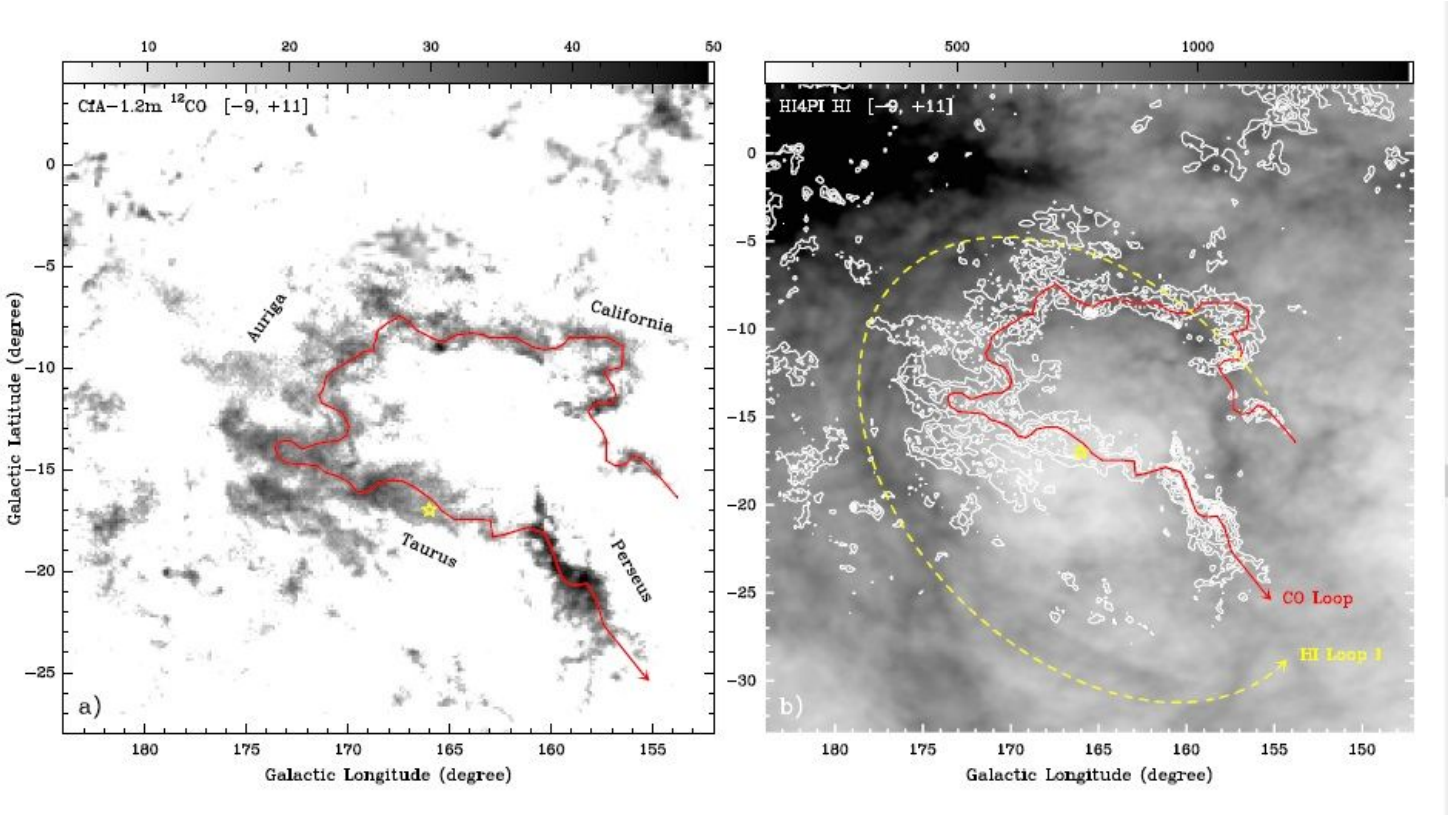

Figure 3

Wide-field CfA 1.2m CO intensity images toward Per OB2. (see Manuscript file for full figure legend)

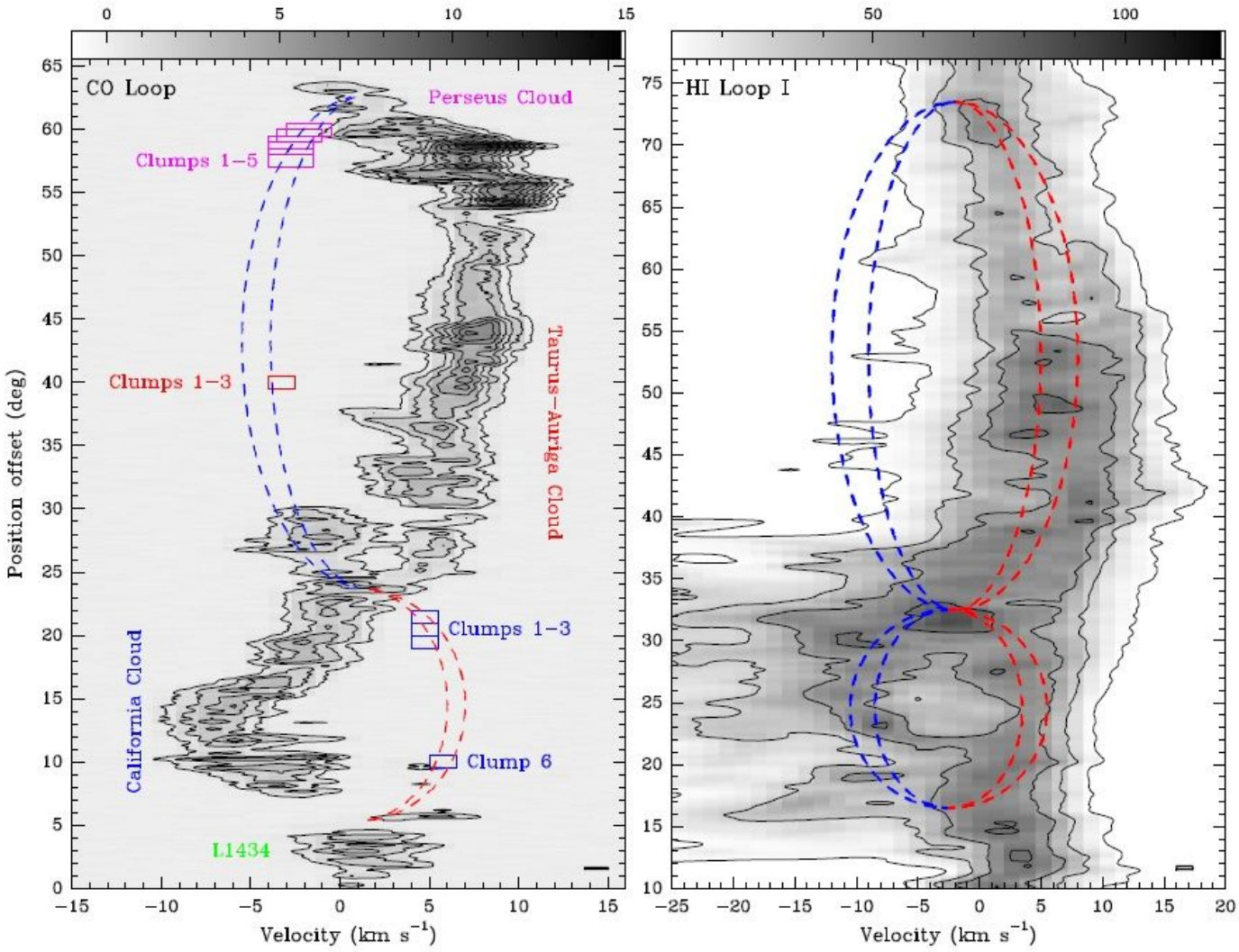

Figure 4

The PV diagrams along the CO loop (left) and HI Loop I (right). (see Manuscript file for full figure legend)